AD-A039 469 BOLT BERANEK AND NEWMAN INC CAMBRIDGE MASS F/G 1/4
DEVELOPMENT OF PROTOTYPE OPTICAL CONVOLUTION AIRSPEED SENSOR.(U)
JAN 77 M J RUDD F33615-76-C-3051
UNCLASSIFIED BBN-3380 AFFDL-TR-76-132 NL

| OF |
AD
A039 469

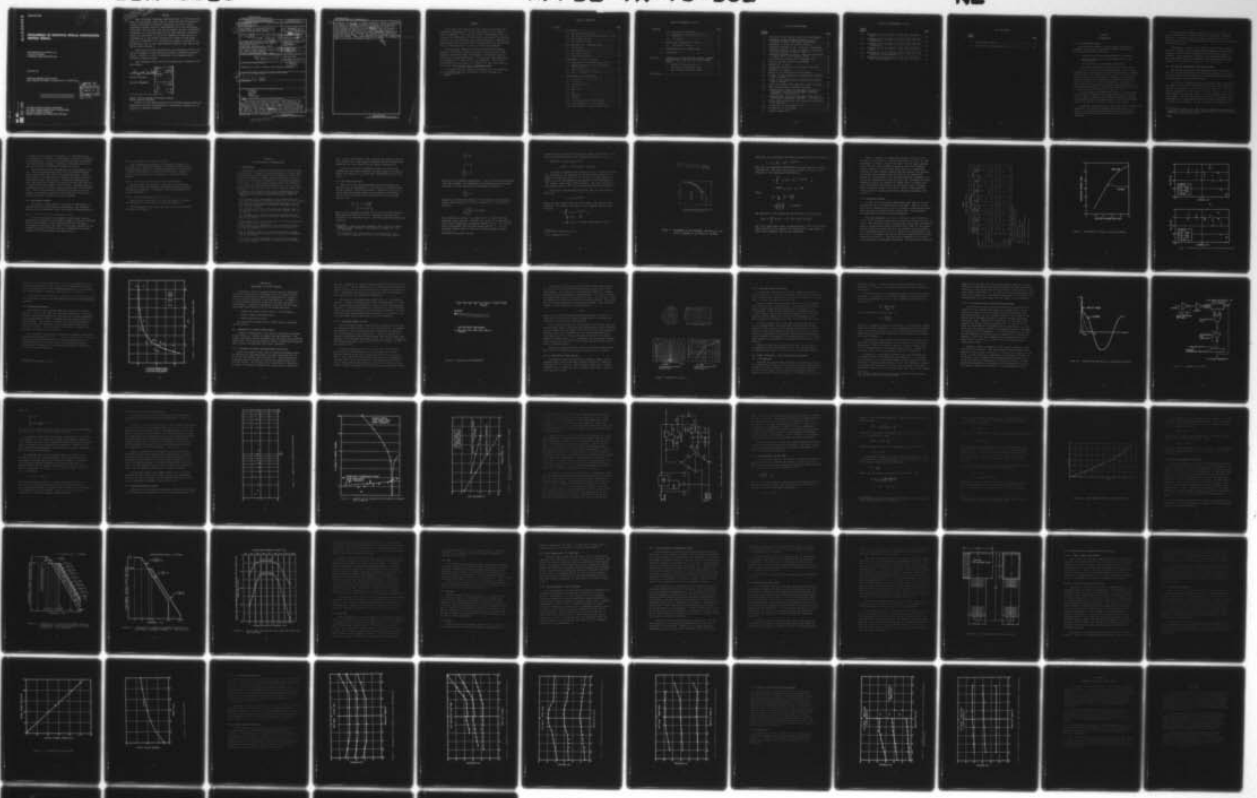

END

DATE
FILMED
6-77

AFFDL-TR-76-132

DEVELOPMENT OF PROTOTYPE OPTICAL CONVOLUTION AIRSPEED SENSOR

BOLT BERANEK AND NEWMAN INC.
50 MOULTON STREET
CAMBRIDGE, MASSACHUSETTS 02138

JANUARY 1977

TECHNICAL REPORT AFFDL-TR-76-132
FINAL REPORT FOR PERIOD 5 JANUARY 1976 - 31 AUGUST 1976

AIR FORCE FLIGHT DYNAMICS LABORATORY
AIR FORCE WRIGHT AERONAUTICAL LABORATORIES
AIR FORCE SYSTEMS COMMAND
WRIGHT-PATTERSON AIR FORCE BASE, OHIO 45433

Correct rept. no. to "3380" per Ms. Dray, BBN, (617) 491-1850 M. Crumbacker TSA - 17 May 77

NOTICE

When Government drawings, specifications, or other data are used for any purpose other than in connection with a definitely related Government procurement operation, the United States Government thereby incurs no responsibility nor any obligation whatsoever; and the fact that the government may have formulated, furnished, or in any way supplied the said drawings, specifications, or other data, is not to be regarded by implication or otherwise as in any manner licensing the holder or any other person or corporation, or conveying any rights or permission to manufacture, use, or sell any patented invention that may in any way be related thereto.

This report has been reviewed by the Information Office (OI) and is releasable to the National Technical Information Service (NTIS). At NTIS, it will be available to the general public, including foreign nations.

This technical report has been reviewed and is approved for publication.

Gary A. DuBro

Project Engineer

FOR THE COMMANDER

ACCESSION for		
NTIS	White Section	☑
DDC	Buff Section	☐
UNANNOUNCED		☐
JUSTIFICATION		
BY		
DISTRIBUTION/AVAILABILITY CODES		
Dist.	AVAIL. and/or SPECIAL	
A		

Chief, Control Systems Development Branch
Flight Control Division

Copies of this report should not be returned unless return is required by security considerations, contractual obligations, or notice on a specific document.

UNCLASSIFIED

SECURITY CLASSIFICATION OF THIS PAGE (When Data Entered)

REPORT DOCUMENTATION PAGE

READ INSTRUCTIONS BEFORE COMPLETING FORM

1. REPORT NUMBER: AFFDL-TR-76-132

2. GOVT ACCESSION NO.

3. RECIPIENT'S CATALOG NUMBER

4. TITLE (and Subtitle): DEVELOPMENT OF PROTOTYPE OPTICAL CONVOLUTION AIRSPEED SENSOR.

5. TYPE OF REPORT & PERIOD COVERED: 5 Jan. 76 ~~(Final)~~ 31 Aug. 76

6. PERFORMING ORG. REPORT NUMBER: ~~BBN-3380~~ 3380

7. AUTHOR(S): M. J. Rudd / Michael J. Rudd

8. CONTRACT OR GRANT NUMBER(S): F33615-76-C-~~3051~~ 51

9. PERFORMING ORGANIZATION NAME AND ADDRESS:
Bolt Beranek and Newman Inc.
50 Moulton Street
Cambridge, Massachusetts 02138

10. PROGRAM ELEMENT PROJECT TASK AREA & WORK UNIT NUMBERS: 62204F 1987 0277

11. CONTROLLING OFFICE NAME AND ADDRESS:
Air Force Flight Dynamics Laboratory
Air Force Systems Command
Wright Patterson AFB, Ohio 45433

12. REPORT DATE: January 1977

13. NUMBER OF PAGES: 79

14. MONITORING AGENCY NAME & ADDRESS (if different from Controlling Office): BBN-3380

15. SECURITY CLASS. (of this report): Unclassified

15a. DECLASSIFICATION/DOWNGRADING SCHEDULE

16. DISTRIBUTION STATEMENT (of this Report)

Approved for public release; distribution unlimited

17. DISTRIBUTION STATEMENT (of the abstract entered in Block 20, if different from Report)

Final rept. Jan–Sep 76,

18. SUPPLEMENTARY NOTES

19. KEY WORDS (Continue on reverse side if necessary and identify by block number)

Airspeed
Velocity
Optics
Turbulence

20. ABSTRACT (Continue on reverse side if necessary and identify by block number)

This report describes the continued development of the Optical Convolution Airspeed Indicator. This relatively inexpensive instrument measures true airspeed by projecting a shadowgraph image of the wake from a small heater onto grating and measuring the ripple frequency of the turbulence crossing the grating. Measurements ~~have been~~ were made on the structure of the turbulent wake so that the heater size and grating can be

→ next page

DD FORM 1 JAN 73 1473 EDITION OF 1 NOV 65 IS OBSOLETE

UNCLASSIFIED

SECURITY CLASSIFICATION OF THIS PAGE (When Data Entered)

060100

cont.

optimized. A new type of signal processor, called a correlation discriminator, ~~has been~~ was developed to measure the frequency of the signal in the presence of a large amount of noise. An active heater protection circuit ~~has been~~ was built to prevent it from burning out when there is no airflow. The effects of environmental conditions on the sensor ~~have been~~ were examined and they can all be met, although the effects of rain and icing require further study. A new improved Prototype ~~Mk II~~ Mark 2 was built and tested. There were significant changes in reading at angles of attack and sideslip above 10 to 15 deg.

PREFACE

This report was prepared by Bolt Beranek and Newman Inc., Cambridge, Massachusetts 02138, under USAF Contract Number F33615-76-R-3051. The objective of this investigation was to continue the development of the Optical Convolution Velocimeter, optimize its optical system and signal processing, consider its environmental suitability, build a second prototype and investigate its susceptibility to angle of attack and sideslip.

This work was supported by Control Systems Development Branch of the Flight Control Division of the Air Force Flight Dynamics Laboratory under "Development of Prototype Optical Convolution Airspeed Indicator." The work was performed under the guidance of G. DuBro and D. Kim AFFDL/FGL. This report was submitted by the author in October 1976 and covers work in the period from January 1976 to September 1976.

The program at Bolt Beranek and Newman Inc. was performed by Dr. Michael Rudd with assistance from N. Westlake and J. Spencer.

TABLE OF CONTENTS

TABLE OF CONTENTS *(CONT'D)*

LIST OF ILLUSTRATIONS

LIST OF ILLUSTRATIONS *(CONT'D)*

LIST OF TABLES

SECTION I

INTRODUCTION

1.1 The Pitot-Static Probe

The Pitot-static probe is the most widely used device for measuring aircraft speed. There are, however, four problems involved with the use of this probe.

- It does not give accurate measurements at low speeds.
- There is a 1/2-second time lag between the probe and the transducer.
- It requires the use of expensive transducers.
- Its analog output must be converted to a digital form.

One port on the Pitot-static probe measures the total impact pressure of the airflow on the probe and another senses the ambient static pressure. The difference between these two pressures is related to the square of the airspeed. However, at low airspeeds (less than about 50 kts) this pressure difference becomes very small and is difficult to measure accurately. Accordingly, in this study we have developed an airspeed sensor based upon a different measurement concept, and which has demonstrated a capability to accurately measure airspeeds at 10 knots or less.

The long pressure line between the Pitot-static probe itself and the pressure transducer which measures the pressure produces a lag of about 1/2 second. An instrument which does not produce this lag would allow the airspeed sensor to follow rapid accelerations of the aircraft or missile on which it was mounted.

In addition, although the Pitot-static tube itself is relatively inexpensive, the pressure transducers associated with it can be costly. A less expensive airspeed sensor that could be used on expendable "remotely piloted vehicles" would be a significant improvement.

The Pitot-tube transducer, which has an analog output that must be converted to a digital format, entails many attendant problems. It would be more convenient and efficient to have a sensor output that is compatible with the digital air data computer on board an aircraft.

Accordingly, G. DuBro and D. Kim* of the Air Force Dynamics Laboratory looked at all the available techniques for measuring airspeed to see if these problems of the Pitot tube could be overcome. They eventually invented a new technique which they have called "The Optical Convolution Velocimeter" and for which a patent (U.S. Patent No. 3,953,126) has been granted.

1.2 The Optical Convolution Velocimeter (OCV)

The optical convolution velocimeter developed by DuBro and Kim+ is a noninvasive method for measuring aircraft speed that eliminates many of the problems encountered with the Pitot-static tubes currently used on board aircraft.

An OCV uses a light-emitting diode (LED) as its light source. The output of the LED is collimated by the lens, and projected through the turbulence onto a grating (see Figure 1). The turbulence is generated by the wake of an object placed in the flow. A mirror behind the grating returns the light through a lens onto a photodiode. As the light passes through the turbulence, it is refracted, and a "shadowgraph" pattern of bright and dark bands is formed on the grating. As the turbulence is convected with

---

* D. Kim and G. DuBro, 1974, "The Optical Convolution Velocimeter" presented at the second Project Squid Workshop, Purdue University, Lafayette, Indiana, March 26-27.

+ Ibid.

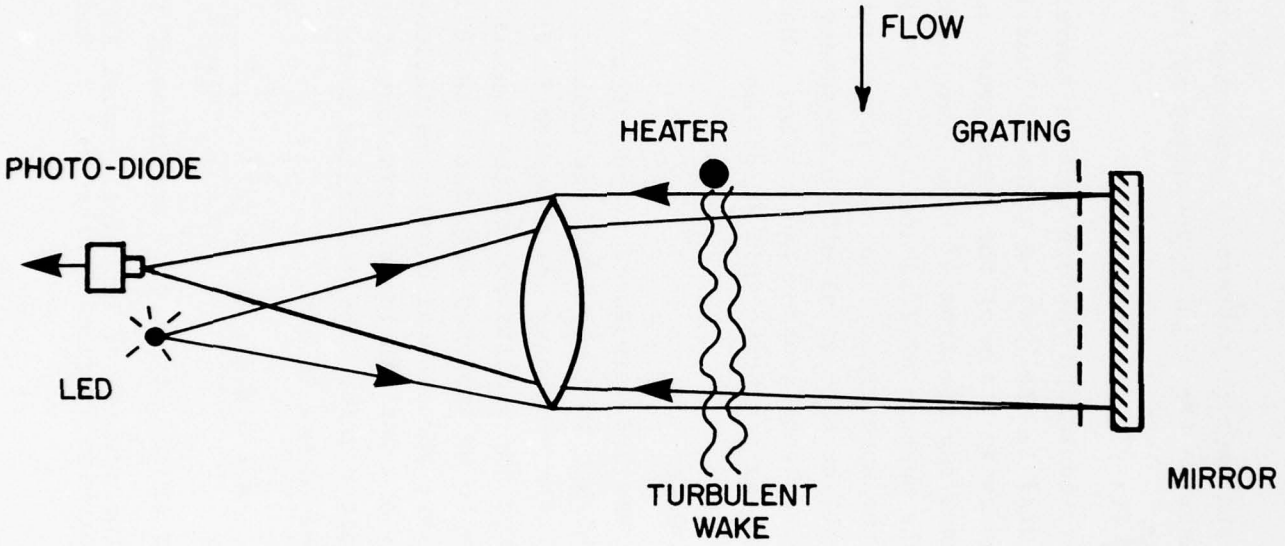

FIGURE 1. PRINCIPLE OF THE OPTICAL CONVOLUTION VELOCIMETER.

the mean flow, the shadowgraph pattern is convected over the grating. We can describe the light transmitted by the grating as

$$\int I(x-y)\ G(x)\ dx = F(y)$$

where I(x-y) is the shadowgraph pattern that is convected in time by distance y, and G(x) is the grating transfer function. The function F(y) is the convolution of the shadowgraph and the grating. By Parseval's theorem, the spectrum of this convolution is equivalent to the product of the spectra of I(x) and G(x). If the spectrum of G(x) is narrow, the spectrum of the convolution function F(y) is narrow, and it will be sinusoidal with a frequency equal to that at which the turbulence crosses the grating. Hence, the velocity can be found by measuring this frequency.

1.3 The Program to Date

In early 1975, the U.S. Air Force awarded Bolt Beranek and Newman the first contract to investigate the feasibility of the OCV as an instrument for measuring low airspeed.* Under that contract, BBN examined the sensitivity of the concept and decided that heat would have to be injected into the flow to increase the instrument sensitivity; the natural density variations due to water vapor and turbulence did not provide a sufficient signal-to-noise ratio with the processor unit. The modulation depth of the light source M was computed to be, in air,

$$M = \alpha\ N\ z_o\ \ 1.4 \times 10^{-3}\ \ \frac{P}{TV(xd)^{\frac{1}{2}}}$$

where N = wavenumber of the light, z_o = thickness of the turbulence,

* This program was the subject of Technical Report AFFDL-TR-75-125 "The Optical Convolution Airspeed Indicator," M. Rudd, November 1975.

P = power per unit length of the heater, T = air temperature, V = airspeed, d = diameter of heater and x = distance of sensitive volume downstream. The factor α describes how well the grating and turbulence are matched. Typically, a modulation depth of 5 parts per million is produced at a speed of 200 mph.

Various light sources and detectors were considered for the OCV. The most suitable were found to be an infrared-emitting diode light source and a silicon photodiode detector. Optics with a speed of f/4 were used to collimate the diode output and a grating of pitch 2 mm was used. A prototype instrument was built and tested on a Cessna 172 aircraft; the unit was flown for 10 hours over a speed range of 50 to 120 mph. Problems were encountered because of the poor signal-to-noise ratio of the instrument. The data was obtained utilizing tape record of the OCV signal, and subsequent analysis of the frequency content with a spectrum analyzer, yielded the measured airspeed.

1.4 The Current Program

The purpose of this report is to relate the development of the OCV during the second stage of the program. The four main tasks which were undertaken during this stage are described below.

Task 1: Definition of Wake Turbulence Spectrum

In the first stage of the program, it was thought that one reason for the relatively weak signal strength was the poor matching of the optical system to the turbulence shed from the heater. Accordingly, measurements were made on the spatial spectrum of the turbulence and its convection velocity to determine the optimum combination of heater diameter and grating pitch.

Task 2: Improvement in Original OCV Design

Some improvements were made to the original OCV design, e.g., the speed of the optics was increased. In addition, a new type of signal processor, called a "correlation discriminator," was developed to measure the frequency of a signal buried in noise. Further, a means of limiting the heat in the absence of cooling airflow was devised.

Task 3: Operational Suitability and Design Specification

The wide range of environmental conditions in which the OCV is likely to operate was considered, and solutions for the potential problems were suggested. A new design of the OCV was made and the new unit fabricated.

Task 4: Testing and Evaluation of the OCV II

This second OCV was tested in the BBN wind tunnel to evaluate its performance for speed, angle of attack, and sideslip.

The performance of these tasks and their results are described in detail in this report.

SECTION II

THE STRUCTURE OF A TURBULENT WAKE

2.1 Introduction

The structure of turbulent wakes has been the subject of many investigations. Although the first measurements of a heated wake were made by Fage and Falkener,* the most extensive studies were performed by Townsend.+ Roshko§ studied the spectra of the turbulence, but was primarily interested in the discrete frequencies in the wake. In a later paper,δ Roshko looked at the turbulence above transition (Reynolds numbers greater than 3×10^5), as did Humphreys.** Tritton∞ examined the flow at Reynolds numbers below

---

* A. Fage and V.M. Falkener, 1935, "Notes on Experiments on the Temperature and Velocity in the Wake of a Heated Cylindrical Obstacle," Proceedings of the Royal Society, Vol. 135A, pp. 702-705.

\+ A.A. Townsend, 1947, "Measurements in the Turbulent Wake of a Cylinder," Proceedings of the Royal Society, Vol. 190A, pp. 551-561.

A.A. Townsend, 1949, "Momentum and Energy Diffusion in the Turbulent Wake of a Cylinder," Proceedings of the Royal Society, Vol. 197A, pp. 124-140.

A.A. Townsend, 1948, "Local Isotropy in the Turbulent Wake of a Cylinder," *Australian Journal of Scientific Research*, Vol. 1A, pp. 161-174.

A.A. Townsend, 1949, "The Fully Developed Turbulent Wake of a Circular Cylinder," *Australian Journal of Scientific Research*, Vol. 2A, pp. 451-468.

§ Anatol Roshko, 1954, On the Development of Turbulent Wakes from Vortex Streets," NACA Report 1191.

δ Anatol Roshko, 1960, "Experiments on the Flow Past a Cylinder at Very High Reynolds Number," *Journal of Fluid Mechanics*, Vol. 10, pp. 345-356.

**John S. Humphreys, 1960, "On a Circular Cylinder in a Steady Wind at Transition Reynolds Number," *Journal of Fluid Mechanics*, Vol. 9, pp. 603-612.

∞ D.J. Tritton, 1959, "Experiments on the Flow Past a Circular Cylinder at Low Reynolds Numbers," *Journal of Fluid Mechanics*, Vol. 6, pp. 547-567.

200. A very comprehensive study, in which the turbulence spectra were studied over a wide range of Reynolds numbers and downstream distances, was more recently done by Uberoi and Freymuth.*

Because the results of Townsend, Roshko, and Uberoi and Freymuth are not always consistent, we have relied on the data of Uberoi and Freymuth as it is the most comprehensive and the most recent.

2.2 Self Preserving Flow

When one is far enough downstream from the cylinder, the turbulent flow is independent of the initial flow conditions and can be scaled in a generalized manner. Townsend+ showed that in the two-dimensional wake behind a long cylinder, the velocity defect u_0 in the center of the wake scaled to the free stream velocity U as

$$\frac{U^2}{u_0^2} = \frac{x}{d} + .043 \left(\frac{x}{d}\right)^{\frac{1}{2}}$$
$$\approx \frac{x}{d} \quad \text{for large } \frac{x}{d}$$

where x is the downstream distance and d is the cylinder diameter. This appears to hold for $x/d > 50$. Similarly, the turbulence velocity u, the turbulence scale L, and the temperature fluctuations θ scale as

---

* Mahinder S. Uberoi and Peter Freymuth, 1969, "Spectra of Wakes Behind Circular Cylinders," *The Physics of Fluids*, Vol. 12, pp. 1359-1363.

+ A.A. Townsend, 1976, *The Structure of Turbulent-Shear Flow* (2nd edition) Cambridge University Press, Cambridge, England.

$$\frac{\overline{u^2}}{U^2} \propto \frac{d}{x}$$

$$L^2 \propto xd$$

$$\frac{\overline{\theta^2}}{T_a^{\,2}} \propto \frac{d}{x}$$

where T_a is the ambient temperature. Thus, as one goes downstream from the cylinder, the turbulence level decreases and its scale increases. On the centerline of the wake, the value of

$$\frac{\overline{U_2}}{u_0^{\,2}} = 0.1$$

according to Uberoi and Freymuth.* In addition, the turbulence spatial spectrum $E_u(k)$ of u^2 is a function of $L = (xd)^{\frac{1}{2}}$ and is given by

$$\frac{E_u(k)}{\overline{U^2}(xd)^{\frac{1}{2}}} = f[k(xd)^{\frac{1}{2}}]$$

This spectrum is flat up to a value of $kL = 6$ and after that decreases quite rapidly. Further, the level of the spectrum is fairly well independent of Reynolds number for $kL < 6$ but varies quite considerably with Reynolds number for $kL > 6$. At low Reynolds numbers there is very little high frequency energy

* Uberoi and Freymuth, op.cit.

because of the destruction of the small eddies by viscosity. The spectra measured by Uberoi and Freymuth* are shown in Figure 2.

Therefore, substituting for $\overline{U^2}$

$$E_u(k) = .1\ U^2\ d(d/x)^{\frac{1}{2}}\ \ f[k(xd)^{\frac{1}{2}}]$$

In trying to maximize this quantity, so as to maximize instrument sensitivity, the quantity U^2 (the free stream velocity) is fixed, k is given the value of 78.5^{-1} in. (12.5 line pairs per inch), and x is determined by the geometry of the instrument at .875 inches. Thus, only d can be varied. The value of $E_u(k)$ is then proportional to $d^{3/2}$ and a spectral density term $f[k(xd)^{\frac{1}{2}}]$.

The velocity distribution across the wake is given approximately by+

$$u = u_0\ e^{-16y^2/xd}$$

where y is the lateral position in the wake. The drag per unit length of the cylinder F is equal to the momemtum defect across the wake

$$F = \int_{-\infty}^{\infty} \rho U\ u_0\ e^{-16y^2/xd}\ dy$$

$$= \frac{\sqrt{\pi}}{4}\ \rho U\ u_0\ \ \sqrt{xd}$$

$$= \frac{\sqrt{\pi}}{4}\ \rho U^2 d, \text{ or a drag coefficient of } 0.89.$$

---

* Uberoi and Freymuth, op.cit.

+ A.A. Townsend, op.cit.

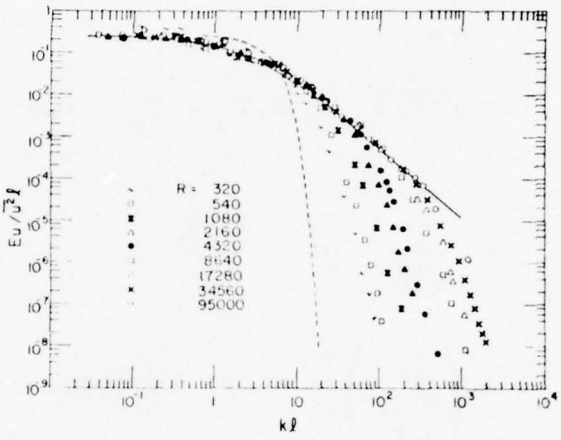

Dependence of the frequency spectra $E_u/\overline{u^2}\,l$ on Reynolds number in the center of the wake.

FIGURE 2. DEPENDENCE OF THE FREQUENCY SPECTRA $E_u/u^2 l$ ON REYNOLDS NUMBER IN THE CENTER OF THE WAKE

Similarly, the temperature distribution across the wake is given by

$$T - T_a = \left(T_o - T_a\right) \quad e^{-10y^2/xd}$$

Note that the temperature distribution is wider than the velocity distribution. The heat flux per unit length P is equal to the integral of the temperature distribution.

$$P = \int_{-\infty}^{\infty} C_p\, U(T_o - T_a) \quad e^{-10y^2/xd} \quad dy$$

$$= \sqrt{\pi/10} \quad C_p\, U(T_o - T_a) \quad \sqrt{xd}$$

Hence,

$$\frac{P}{F} = \frac{4}{\sqrt{10}} \quad \frac{C_p}{P} \quad \frac{T_o - T_a}{U_0}$$

$$\approx \left(\frac{\overline{\theta^2}}{\overline{u^2}}\right)^{1/2} \quad \text{, by analogy.}$$

The spectrum of the temperature fluctuations is then given by

$$E_\theta(k) = \frac{\theta^2}{\overline{u^2}}\, E_u(k) = .1\, \overline{U^2} \quad \frac{P}{F}\, d\, (d/x)^{1/2}\, f[k(xd)^{1/2}]$$

and, for a given heat input, is proportional to $d^{3/2}$ and $f[k(xd)^{1/2}]$. Since $f[k(xd)^{1/2}]$ falls rapidly for large $k(xd)^{1/2}$, large values of this latter parameter need not be considered.

Table 1 compares the turbulence spectral levels for five different wire sizes for a spatial wavenumber of 78.5^{-1} in. and a distance of .875 in. behind the wire. For the three smallest wires there is little change in spectral level with Reynolds number; however, for the larger wires there is a significant decrease at lower Reynolds numbers and accordingly, the spectral levels have been computed for both ends of the speed range. Generally, the spectral levels increase with wire diameter, even though the nondimensional spectrum $E_u/u^2 \sqrt{xd}$ decreases with wire diameter, because the spectrum of larger wires is spread over fewer wavenumbers and because the turbulence level is higher, being relatively closer to the wire. On the other hand, the velocity defect increases as the wire diameter increases (see Figure 3).

2.3 Turbulence Spectra

As part of this program, measurements were made of the turbulence spectra in the wake behind a cylinder. Rods of 1/4-in. and 1/8-in. diameter were set up in the BBN low speed wind tunnel which was run at speeds between 6 and 45 mph. The turbulence was measured with a DISA hot wire anemometer.

The data presented in Figures 4 through 6 cover distances from 2 to 64 diameters downstream and Reynolds numbers from 650 to 9,500. The horizontal axis is the Strouhal number and the vertical axis is the spectral density divided by $\overline{u^2}d$, where $\overline{u^2}$ is the mean square turbulent velocity and d is the diameter of the cylinder. At a downstream distance of x = 2, there is a 10-dB spread in the data, but it collapses much better farther downstream for Strouhal numbers less than 0.2. Discrete vortex shedding is not visible more than about 16 diameters downstream. The spectra are typically

TABLE 1

WAKE SPECTRAL LEVELS

	Wire Diameter						
	.0063	.01	.02	.03		.04	
	10-300 mph	10-300 mph	10-300 mph	10 mph	300 mph	10 mph	300 mph
$\sqrt{xd}$ in	0.074	0.094	0.132	0.162	0.162	0.187	0.187
$k\sqrt{xd}$	5.8	7.4	10.4	12.7	12.7	14.6	14.6
Re (10 mph)	57.6	91.4	182.7	275.0	--	365.0	--
Re (300 mph)	1728.0	2742.0	5481.0	--	8250.0	--	10950.0
$E_u/u^2\sqrt{xd}$	5.0×10^{-2}	3.0×10^{-2}	2.0×10^{-2}	7.0×10^{-3}	1.5×10^{-2}	4.0×10^{-3}	1.2×10^{-2}
$\overline{u^2}/U^2$	7.0×10^{-4}	1.2×10^{-3}	3.6×10^{-3}	7.5×10^{-3}	7.5×10^{-3}	1.2×10^{-2}	1.2×10^{-2}
E_u/U^2	2.6×10^{-6}	3.4×10^{-6}	9.5×10^{-6}	8.5×10^{-6}	18.0×10^{-6}	9.0×10^{-6}	27.0×10^{-6}
10 log (E_u/U^2)	-55.8	-54.6	-50.2	-50.7	-47.4	-50.5	-45.7
Velocity Defect	8.5%	10.7%	15.1%	18.5%	18.5%	21.4%	21.4%

$k = 78.5^{-1}$ in., wavenumber of grating

$x = .875$ in., downstream distance

d = wire diameter

$\sqrt{xd}$ = scale of turbulence

Re = Reynolds number

E_u = energy spectral density

$\overline{u^2}/U^2$ = turbulence intensity

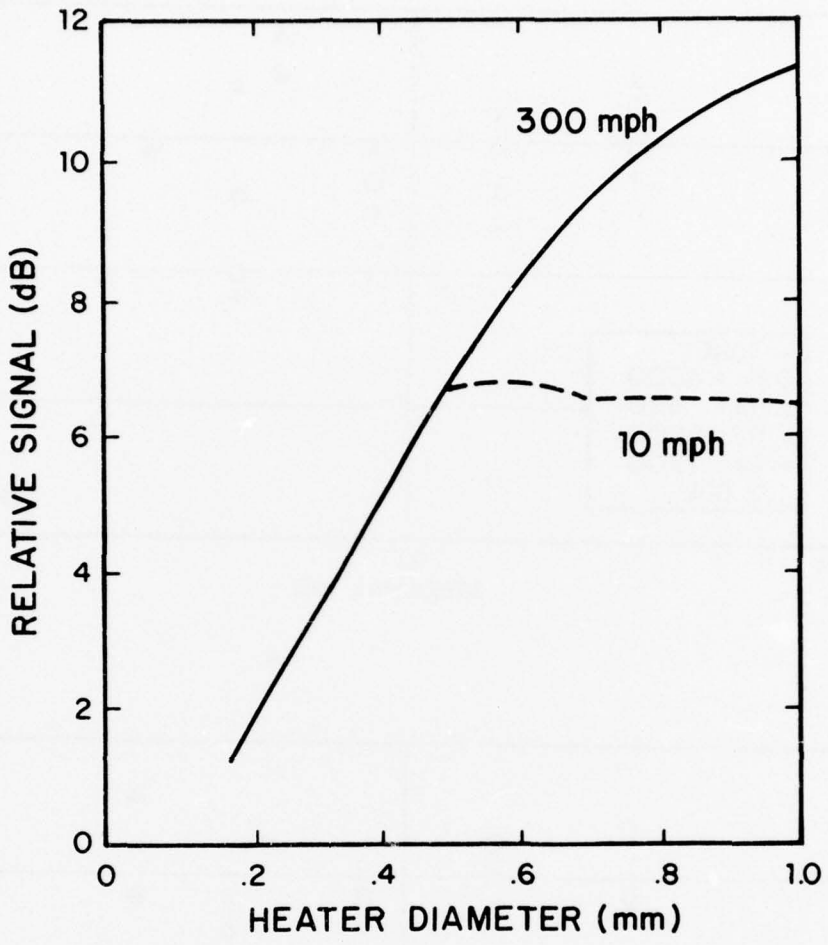

FIGUR E 3. DEPENDENCE OF SIGNAL ON HEATER DIAMETER

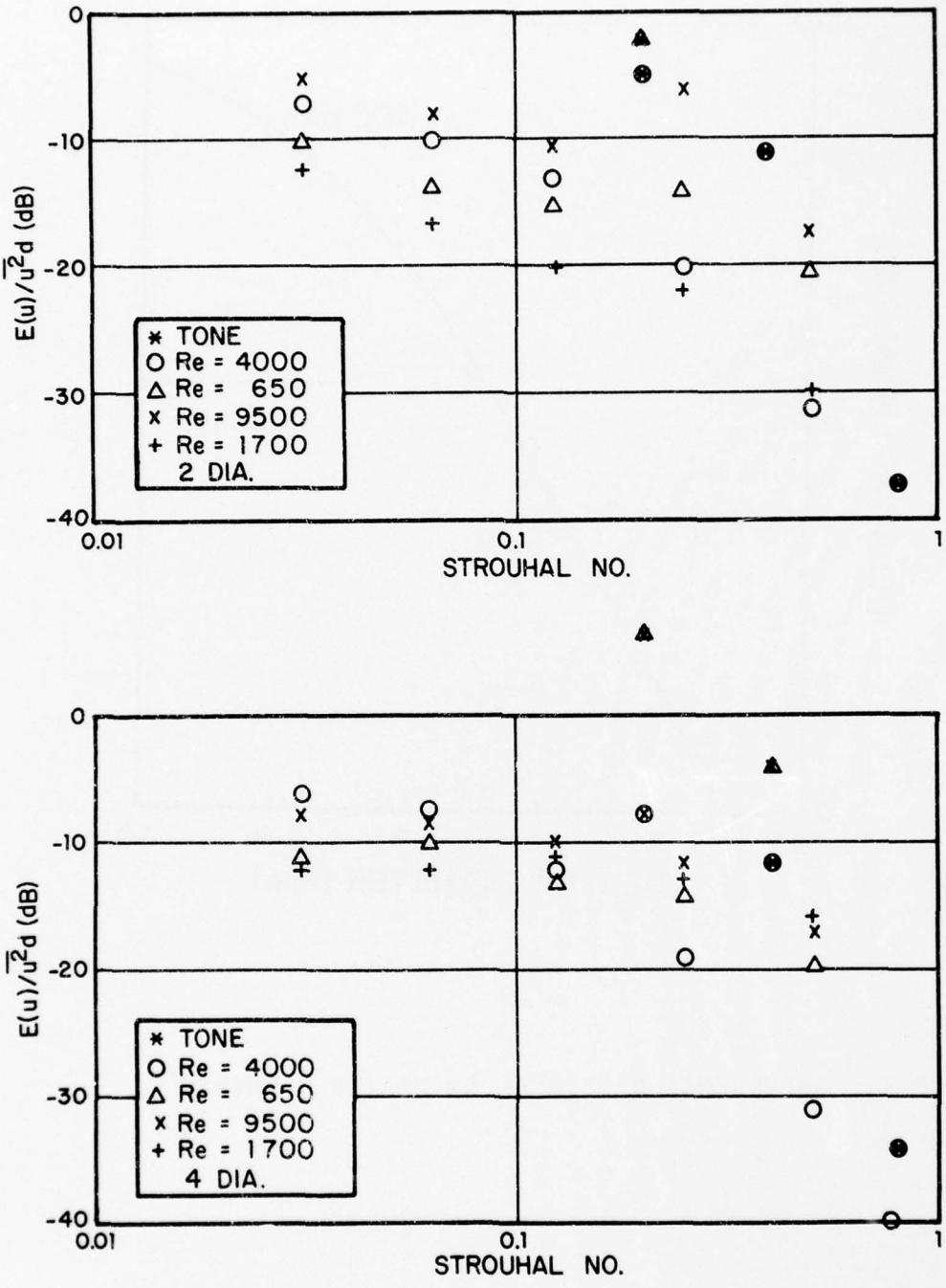

FIGURE 4. TURBULENCE SPECTRA (2 and 4 diameters downstream).

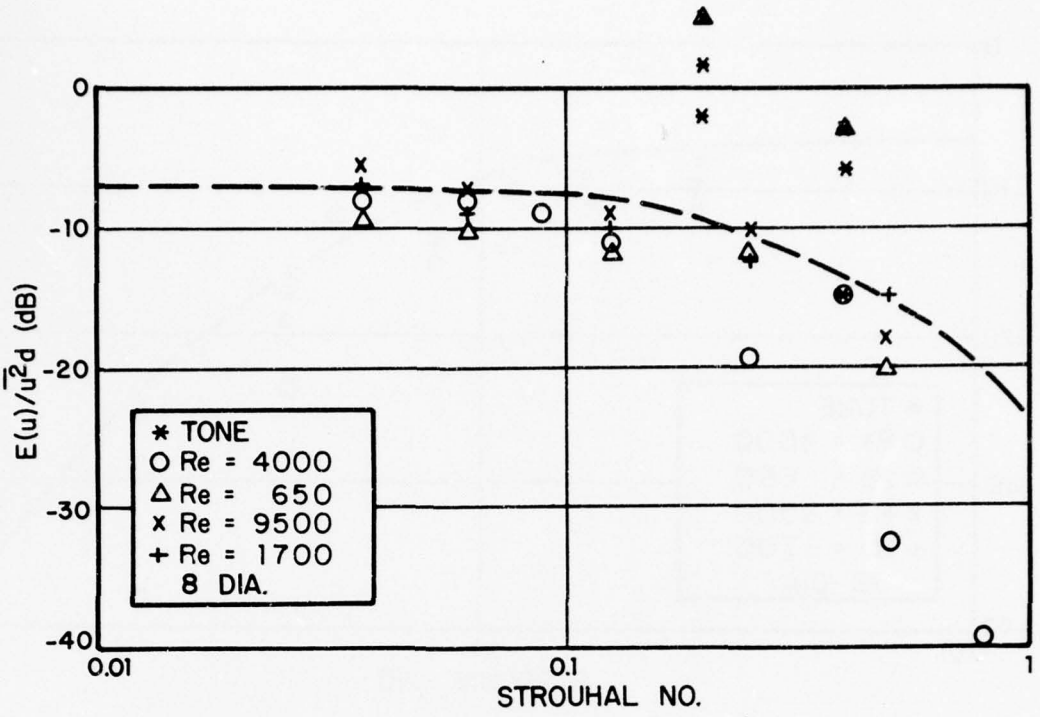

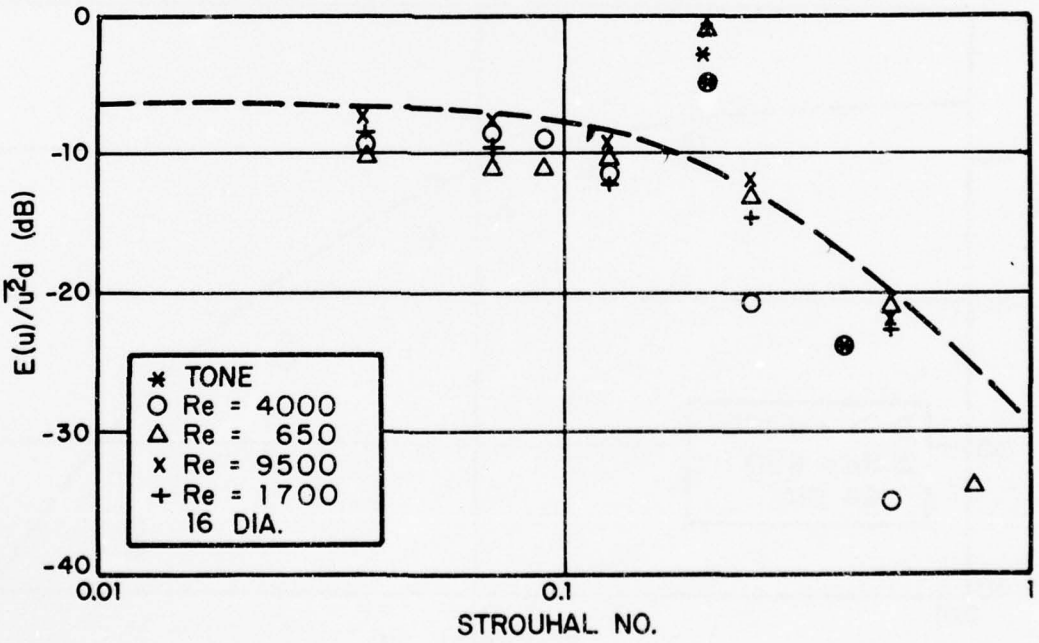

FIGURE 5. TURBULENCE SPECTRA (8 and 16 diameters downstream) [After Uberoi and Freymuth, 1969].

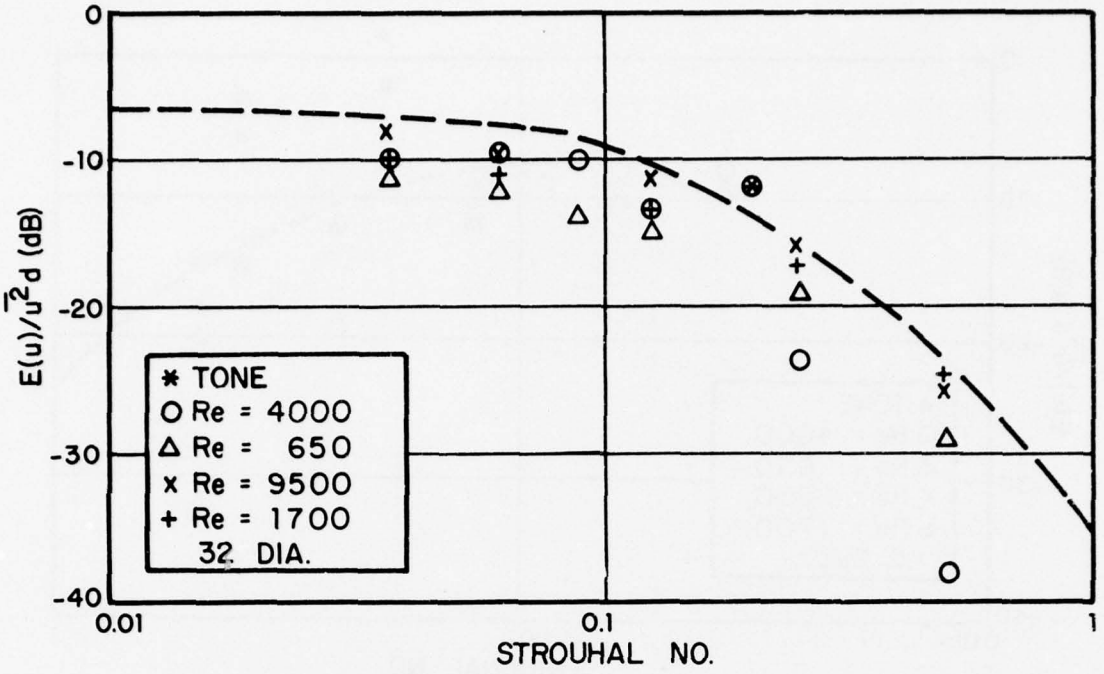

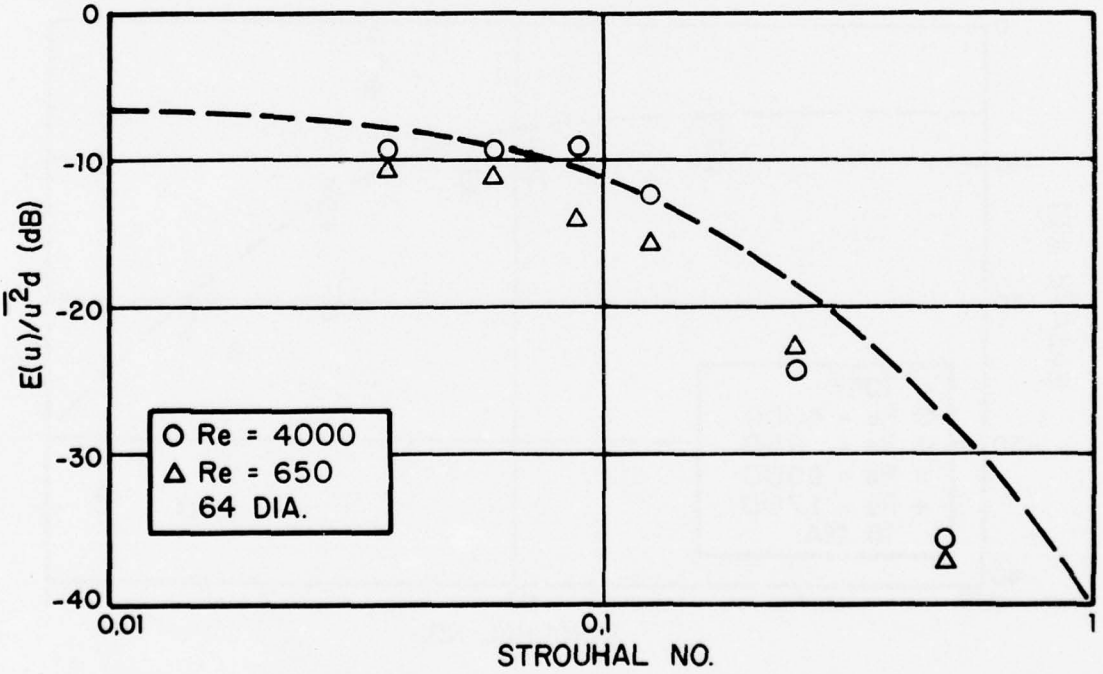

FIGURE 6. TURBULENCE SPECTRA (32 and 64 diameters downstream) [--After Uberoi and Freymuth, 1969].

flat, out to a Strouhal number of 0.1 to 0.2, and then fall off as approximately the inverse fourth (-11/3 theoretically) power of the Strouhal number. The broadband spectrum at x = 4 is about one octave higher in frequency than that at x = 32 or 64.

The dotted lines in Figures 5 and 6 are the spectra computed from the paper by Uberoi and Freymuth* and are shown for comparison purposes.

2.4 Convection Velocity

The eddies in the turbulent wake are convected at a speed which is a little less than the free stream velocity. This convection velocity was measured by mounting two hot wire anemometers in the wake behind a 1/4-in. cylinder and then cross-correlating their outputs. The delay in the peak of the cross-correlation function gives the convection time of the eddies from one hot wire to the other. The convection velocity can be obtained by measuring the spacing of the wires.

The convection velocity as a function of distance downstream from the rod is shown in Figure 7. Close to the rod, the convection velocity is significantly below the free stream velocity, but farther downstream it is very close to free stream velocity. Beyond about 35 diameters, the convection velocity is within 3% of the free stream velocity.

---

* Uberoi and Freymuth, op.cit.

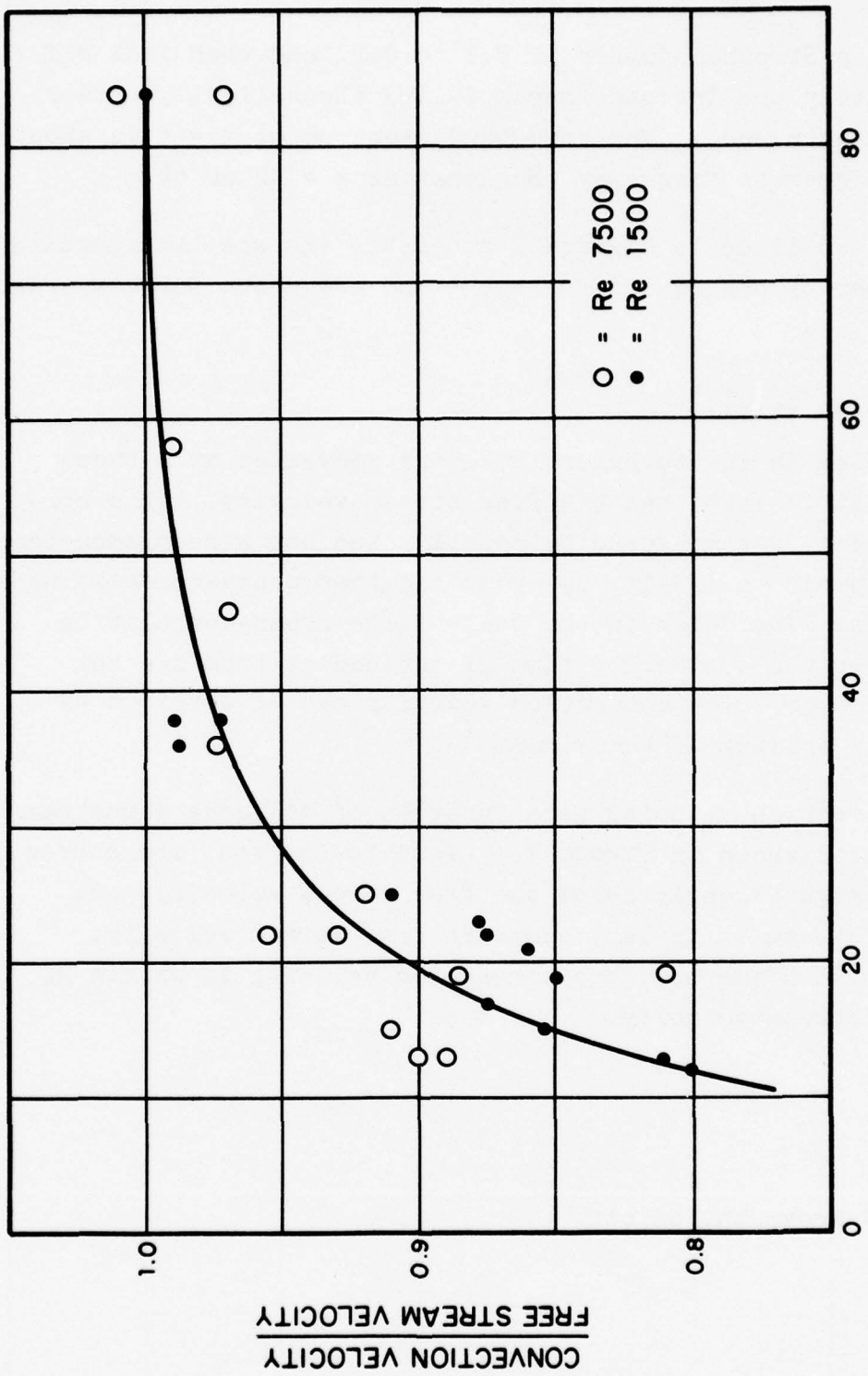

FIGURE 7. THE CONVECTION VELOCITY IN A TURBULENT WAKE.

SECTION III

IMPROVEMENT IN THE OCV DESIGN

Although the first prototype OCV which had been fabricated during the first contract, performed well, its signal-to-noise ratio was insufficient to measure the frequency by a counter; it could only be measured by a spectrum analyzer. In addition, at low airspeeds the heater became very hot and even glowed. Accordingly, a program was undertaken to improve the OCV design and remedy these factors, with the following objectives.

- Improve the signal-to-noise ratio of the instrument.
- Design a signal processing system.
- Provide heater protection.

The significant progress made in these areas is described in this section.

3.1 Improvement in Signal-to-Noise Ratio

A number of alterations to the optical system were considered in our efforts to increase the signal from the instrument. The changes considered included increasing the LED output and photodiode sensitivity, increasing the number of LED's, considering alternative light sources, and improving the optical efficiency.

3.1.1 Increased LED output and photodiode sensitivity

There are currently three LED's of similar performance which are suitable for this application; the Texas Instruments TIL 31 or 34, the RCA SG1009A, and the GE SSL 55C. They generally have a minimum output of 5 mwatt at 100 ma drive current (with less from the TIL 34). The GE device can be overdriven to 300 ma for an output of 14 mwatt, providing that a heat sink is attached to

the case. However, all devices must be derated if they are to be used at 125°C. The SG 1009A and TIL 34 can be driven at 50 ma and the SSL 55C at 0 ma at 125°C, and the TIL 31 cannot be used above 80°C. Therefore, the output of the LED can only be increased at the expense of its top operating temperature.

The original photodiode had a sensitivity of .35 amp/watt. However, a number of manufacturers have increased this to .6 amp/watt by applying an antireflection coating to the silicon photodetector. A further improvement in sensitivity of the instrument can be achieved by employing a high impedance amplifier. In fact, a suitable photodiode-preamplifier combination is available from Bell and Howell and is being used for this instrument.

3.1.2 Increased number of LEDs

Since the power output from an LED is limited, the only way to obtain more light output is to use multiple LEDs. An arrangement similar to the dual detector OCV, only using two LEDs and one photodetector, is one possibility. However, because the velocity signal would have opposite phase from the two LEDs, when added by the photodiode they would cancel each other. In addition, the system would have similar difficulties of alignment as the dual detector OCV.

Another arrangement would be to have two light emitting diodes and two photo-diodes lie at the corners of a square. Each photo-diode would then receive the light from one of the LED's. The outputs of the two photo-diodes would be summed and we would have a 3 dB improvement in the signal-to-noise ratio over a single LED/photo-diode pair. There would not be any increase in power consumption if the LED's were connected in series.

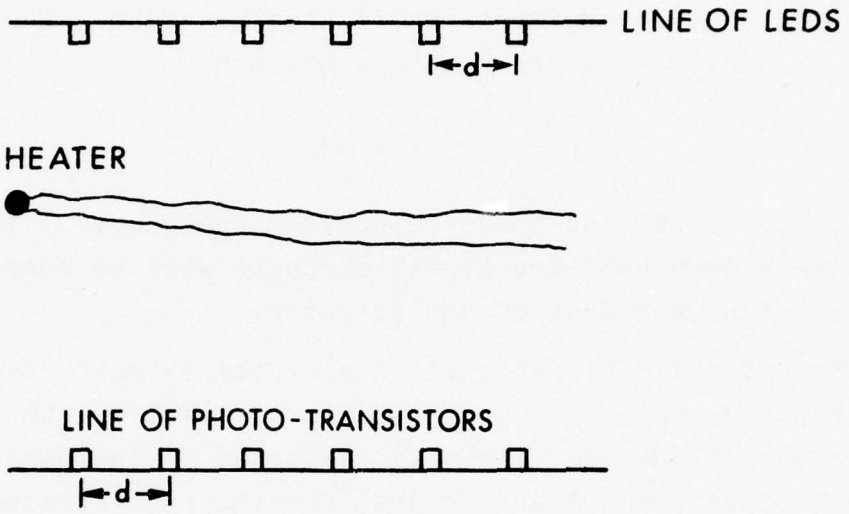

Figure 8. MULTIPLE LED VELOCIMETER.

A completely different type of optical system would consist of a line of LED's and photodetectors along either side of the flow channel. This system is illustrated in Figure 8. Strings of LED's and photo-transistors are available on 0.1 inch centers for paper tape readers (for example TIL 133). All the LED's would be connected in series and driven at the same current. The output of all the photo-transistors would also be added. The frequency output, f, for a velocity v is now given by

$$f = v/d$$

where d is the LED and photo-transistor spacing (0.1 inch). If there are n detectors the signal strength will be increased by a factor of n over that of one detector.

The optical efficiency of this system is much lower than the ones proposed above. Since the LED's are smaller, their beamwidth is much larger and less light is collected by the phototransistor. Further, since the collecting lens for the photo-transistor is very small, much less light is collected than with the single large collimating lens. It is estimated that the signal strength will be only one tenth that of the single LED/photo-diode system with a collimating lens.

This system may have value, however, when an extremely compact system is required and signal strength is not a problem.

3.1.3 Alternative light sources

Alternative light sources such as tungsten lamps, quartz halogen lamps, and low and high pressure mercury arc lamps are discussed in the appendix. Small tungsten lamps have a signal strength close to LEDs but have a larger source size, a shorter life, and are bulkier.

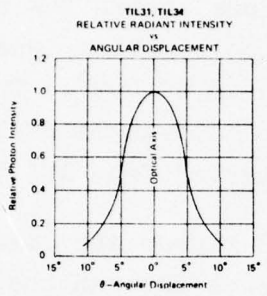

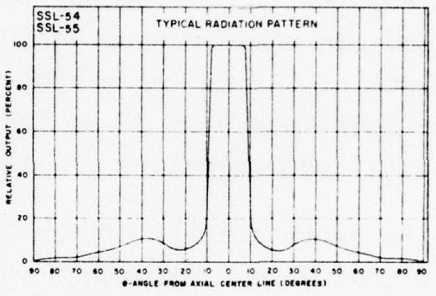

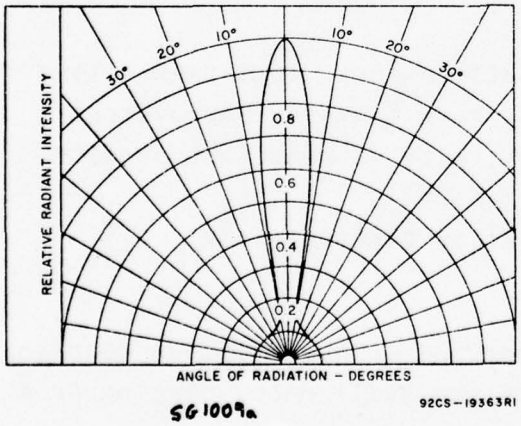

SG 1009a

Typical Radiant Intensity vs Angle From Central Axis of Diode

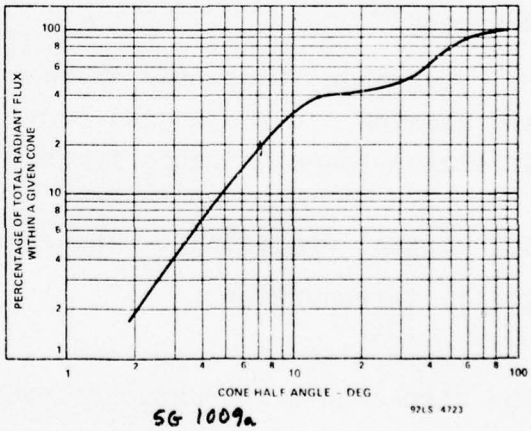

SG 1009a

Percentage of Total Radiant Flux Within a Given Cone Angle

FIGURE 9. DIRECTIVITY OF LEDs

3.1.4 Improved optical efficiency

A significant improvement in optical efficiency was made in the OCV design by (1) shortening the focal length of the collimating lens to collect more light from the LED, and (2) reducing the stray light to reduce the shot noise on the LED.

Figure 9 shows the directivity of the three LED's considered. They range from 5° to 10° half-angles. Also shown is the percentage of output light collected by various cone angles for the SG 1009A LED. In the previous design, the collimating lens had a focal length of 132 mm for a cone half-angle of 6.9°. The new lens has a focal length of 82 mm for a cone half-angle of 11°. This increases the percentage of light collected from 19% to 33%.

Only the central parts of the lens and mirror are covered by the turbulent wake. The light which passes through the edge regions is still returned to the photodiode and there it contributes to the shot noise which is the main source of noise in the detector. Accordingly, the original circular reflective grating (32 mm diameter) was changed to a rectangular grating (12 x 32 mm), which produced an approximate 3-dB reduction in shot noise in the detector.

Together, these two optical modifications, of a faster lens and masking out the unused portions, give a 5.4 dB improvement in signal-to-noise ratio for the OCV, with no resultant penalty.

3.2 Signal Processing: The correlation Discriminator

3.2.1 Introduction

Even with the improvements described in the previous sections, the signal-to-noise ratio of the OCV was still poor, ranging from +10 dB to -10 dB. In addition, the signal frequency can range over at least a 30:1 range. On the original instrument, a spectrum analyzer was used to measure the peak of the signal spectrum in the

presence of noise. However, this was slow, expensive, and not automatic. Therefore, an alternative method of signal processing was needed.

A counter was first considered as a way to measure the signal frequency. The count N for a signal frequency f, in the presence of noise of bandwidth bf ($b \geq 1$), and a signal-to-noise ratio, ρ, is given by*

$$\frac{N}{f} = \left(\frac{\rho+b^2/3}{\rho+1}\right)^{\frac{1}{2}}$$

or for small errors in the count N

$$\Delta N \approx \frac{b^2/3-1}{2(\rho+1)}$$

Thus, for a frequency range of 30:1 and for a 1% accuracy a signal/noise of 15 dB is required at the top frequency and a 42 dB signal/noise at the lowest frequency. The OCV does not have this high signal-to-noise ratio and, therefore, such accuracy is not achievable with a counter.

A phase-locked loop, which is often proposed as optimal technique for frequency measurement, is not suitable for the present application. This is because in order to capture a signal over a 30:1 frequency range, its bandwidth must be made so large that it cannot lock on to the weak signal that the OCV produces.

Accordingly, a new signal processor has been developed and is referred to as the "Correlation Discriminator." Its purpose is the detection of a sinusoidal signal in the presence of white noise with a signal-to-noise ratio $\geq$ 0 dB. The technique is based on automatically measuring the first zero crossing of the autocorrelation function of the combined signal and noise. This method

---

*J.S. Bendat, 1958, *Principals and Applications of Random Noise Theory*, John Wiley and Sons, New York.

makes use of the fact that the autocorrelation function of white noise is a spike centered at zero time delay and that, therefore, it does not distort the correlation function of the signal at other time delays (see Figure 10). We compute the auto-correlation function of the signal at a time delay long enough for the noise to be uncorrelated, but short enough for the signal to be correlated.

3.2.2 Principle of the correlation discriminator

The correlation discriminator computes the autocorrelation function of the clipped input signal at a single time τ by delaying the signal in time (by means of a shift register) and then multiplying it by the undelayed signal. The output of the multiplier is averaged and used to drive a voltage controlled oscillator (VCO). This VCO is used in turn to clock the shift register and hence, forms a feedback loop. If the VCO is too high, the autocorrelation function will be computed at τ_1. The value will be positive and thus the integrator output is arranged to decrease the VCO frequency. If the VCO frequency is too low, the autocorrelation function will be computed at τ_2 and will be negative. This time the integrator will increase the VCO frequency until a value of τ_0 is then 1/4 of the period of the incoming sine wave.

Figure 11 shows a schematic of the circuit required to perform the above function. The input signal passes through a preamplifier whose primary purpose is to "whiten" the spectrum of the noise. If the noise has a significant low frequency content, or is "pink", it will lengthen the autocorrelation function of the noise and distort the sinusoidal correlation function. Accordingly, the preamplifier attenuates the low frequency noise until its spectral components are equal to the high frequency noise.

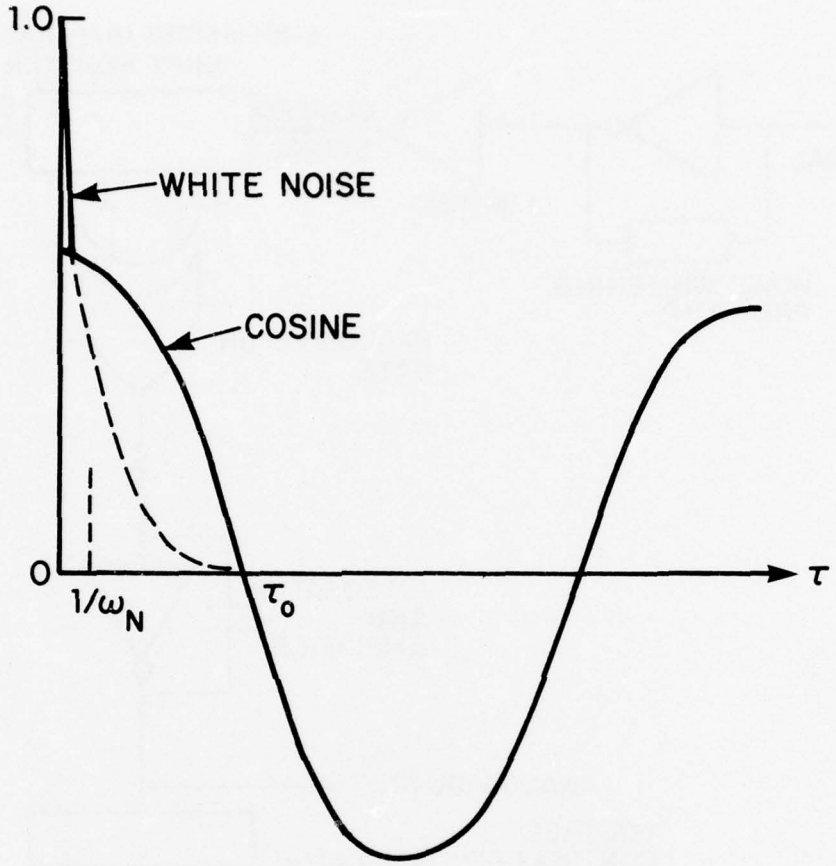

FIGURE 10. CORRELATION FUNCTION OF A SINE WAVE PLUS NOISE

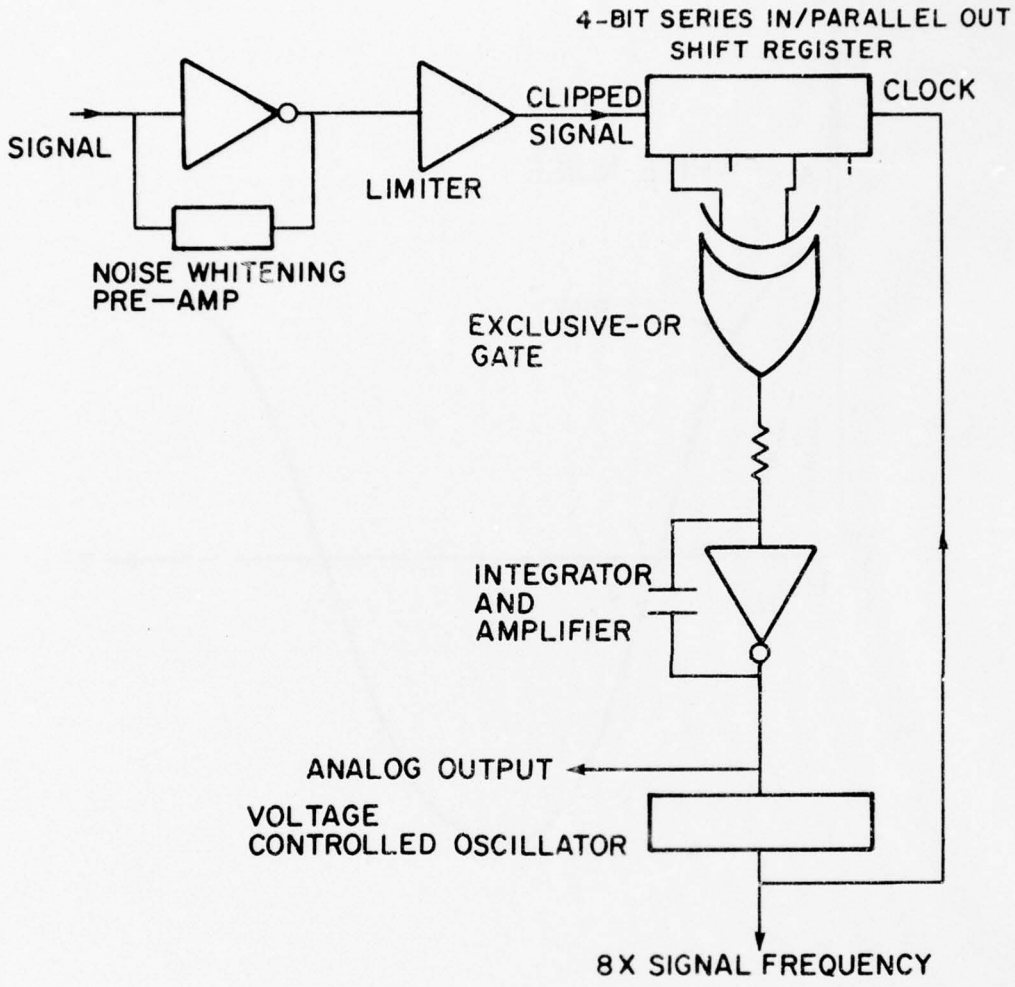

FIGURE 11. SCHEMATIC OF CIRCUIT

Too much attenuation, however, can cause the autocorrelation function of the noise to go negative, and can produce as severe an error as could be experienced with too little attenuation. A flat noise spectrum is optimal.

The next circuit element is a limiter which clips the signal and is, in effect, a one-bit digitizer. This greatly improves the ease of multiplication and the levels of confidence of the autocorrelation function. It does this at the expense of degrading the signal-to-noise ratio by a factor or $\pi/4$ or 1 dB.

The clipped signal next passes into a variable delay line which comprises a 4-bit, serial-in, parallel-out, shift register controlled by a variable clock. The first and third outputs from the shift register are multiplied together by an Exclusive-Or (EXOR) gate which performs as a one-bit multiplier. The output of the gate is then integrated by an analog integrator with a preset time constant of about 1/10 second. The integrator has a voltage gain of about 100 in order to minimize the error in sensing the zero crossing of the autocorrelation function. The output of the integrator is used to control a VCO which in turn is the clock for the shift register.

The last three components (the multiplier or EXOR gate, the integrator, and the VCO) are the basic components of a phase-locked loop and are available as one integrated circuit. However, a phase-locked loop does not employ a shift register, and multiplies the signal and VCO together directly.

Two outputs are available from this circuit: a digital output from the VCO which runs at 8 times the input frequency, or an analog output from the integrator.

When the circuit is first switched on, there will be no sinusoidal signal present, only noise. In this case, the circuit will lock on to the zero crossing of the noise autocorrelation function which will cause the VCO to be driven to its *highest frequency;* hence, this loss of signal can be diagnosed. An alternative condition is loss of both signal and noise from the input. Then the outputs of the shift register will always have the same level, independent of frequency, and the VCO will be driven to its *lowest frequency* which will also diagnose this condition.

3.2.3 Theory of the signal analysis technique

Let us consider a sinusoidal signal in the presence of noise with a power spectrum of the form

$$\frac{N}{1 + (\omega/\omega_n)^2} + S\ \delta(\omega-\omega_s) \quad ,$$

where ω_n and ω_s are the bandwidth of the noise and the frequency of the signal, respectively. The autocorrelation of the signal is then

$$N \exp(-\omega_n\tau) + S \cos(\omega_s\tau) \quad .$$

We shall now seek the first zero crossing of $\cos(\omega_s\tau)$. However, in practice, we will measure the zero crossing of the above correlation function. The error is then

$$\frac{\Delta\tau}{\tau} \approx \frac{2}{\pi}\frac{N}{S} \exp(-\pi\omega_n/2\omega_s) \quad .$$

Thus, for

$$\frac{\Delta\tau}{\tau} = 1\%$$

$$\frac{\omega_n}{\omega_s} = \frac{2}{\pi} \ln\left(\frac{N}{S}\right) + 2.644 \quad .$$

Therefore, for a signal-to-noise ratio of 0 dB, the noise bandwidth must be at least 2.644 times the signal frequency.

It should be noted that this theory is dependent on the noise being "white." If the noise has a large low frequency component, or is "pink", the tail of the correlation function will be increased and the accuracy of the system will be degraded. Therefore, the noise should be prewhitened by attenuating low frequency components before they enter the analyzer.

The sampling rate of the incoming signal is equal to the frequency of the VCO. This frequency f is $4n\ \omega_s/2\pi$, where n is the number of delays employed in the shift register. According to the Shannon sampling theorem, this sampling rate must be greater than twice the highest frequency to be sampled, which is the noise bandwidth of 2.644 times the highest signal frequency $\omega_s/2$. Therefore,

$$f = 4n > 5.288\ \omega_s/2\pi \quad .$$

The smallest integral value of n which satisfies this is n = 2, thus, at least two delays must be used in the shift register; more delays will produce a somewhat higher accuracy at the expense of a higher oscillator frequency. With n = 2, the oscillator frequency is 8 times the highest signal frequency.

Testing the Correlation Discriminator

A number of tests have been performed on the correlation discriminator and their results are summarized in Figures 12, 13 and 14.

In Figure 12, the absolute error of the correlation discriminator is plotted over a frequency range of 1.2 to 100 kHz. The signal-to-noise ratio was +10 dB. The maximum error is +0.3% with a mean error of +0.2%, which is a very impressive accuracy. For comparison, the theoretical error of a zero-crossing counter is compared with the correlation discriminator for the same signal-to-noise ratio. Except at a frequency of $1/\sqrt{3}$ of the noise bandwidth (the count due to noise alone, thus no error) the counter has a very poor accuracy. (See Figure 13.)

Figure 14 compares the fluctuations of the correlation discriminator and those theoretically expected for a counter. The count is for 12,500 cycles of the signal frequency. The correlation discriminator is substantially steadier than the counter primarily because of the extra integration in the circuit. At 0-dB signal-to-noise, there is only 0.3% fluctuation and at +20 dB signal-to-noise only a 0.001% fluctuation.

The circuit handles input signals from 1 mV to 5 V, and frequencies from 1.2 kHz to 100 kHz, without any adjustement. In fact, the only adjustment is the comparator offset and this is not necessary for signals of more than 10 mV.

3.3 Heater Protection Circuit

The heater on the original instrument consisted of a length of Nichrome wire through which a steady current was passed. The

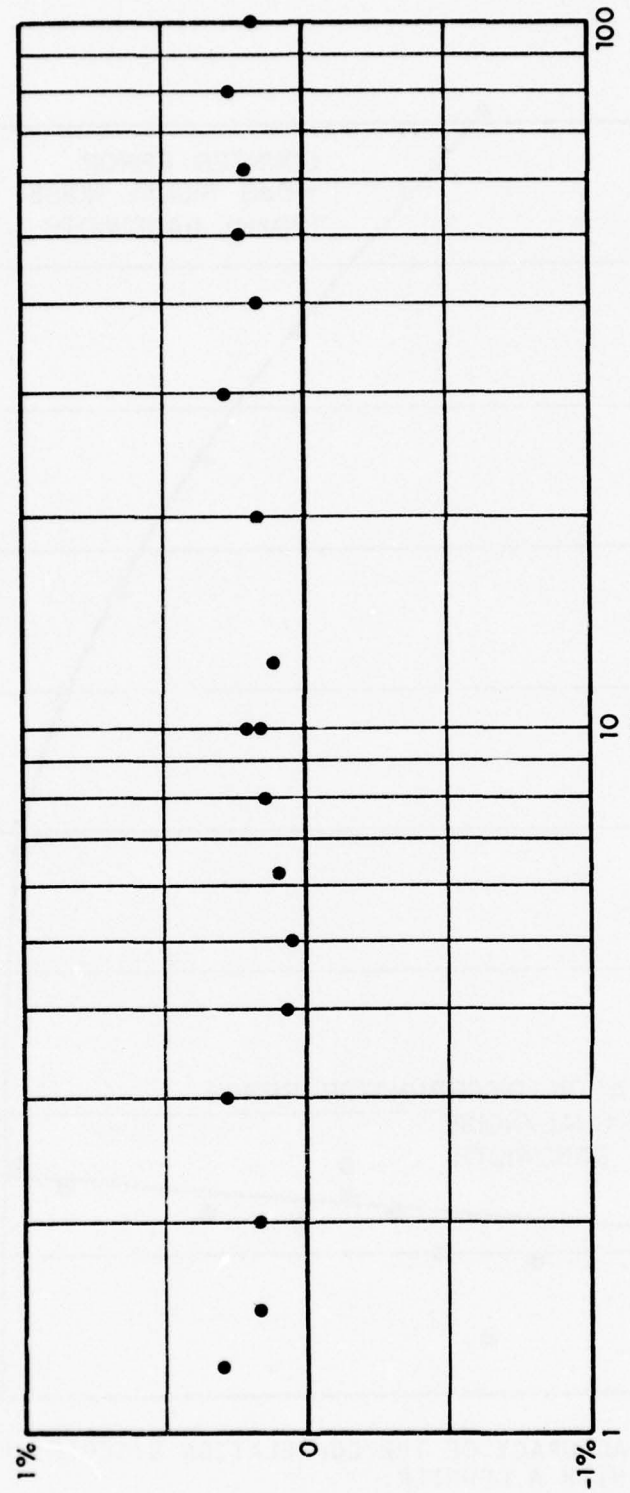

FIGURE 12. ERRORS IN THE CORRELATION DISCRIMINATOR.

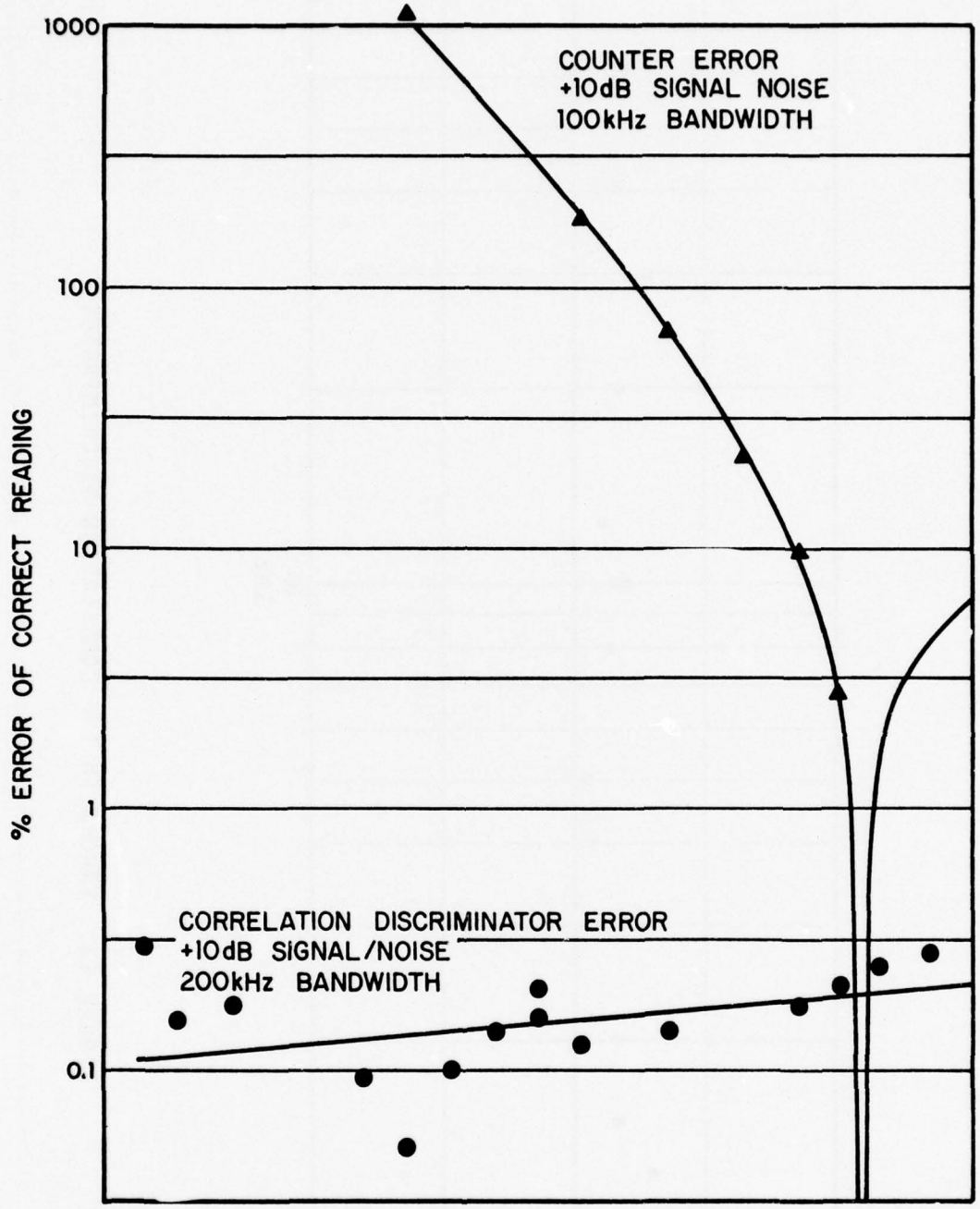

FIGURE 13. ACCURACY OF THE CORRELATION DISCRIMINATOR COMPARED WITH A COUNTER.

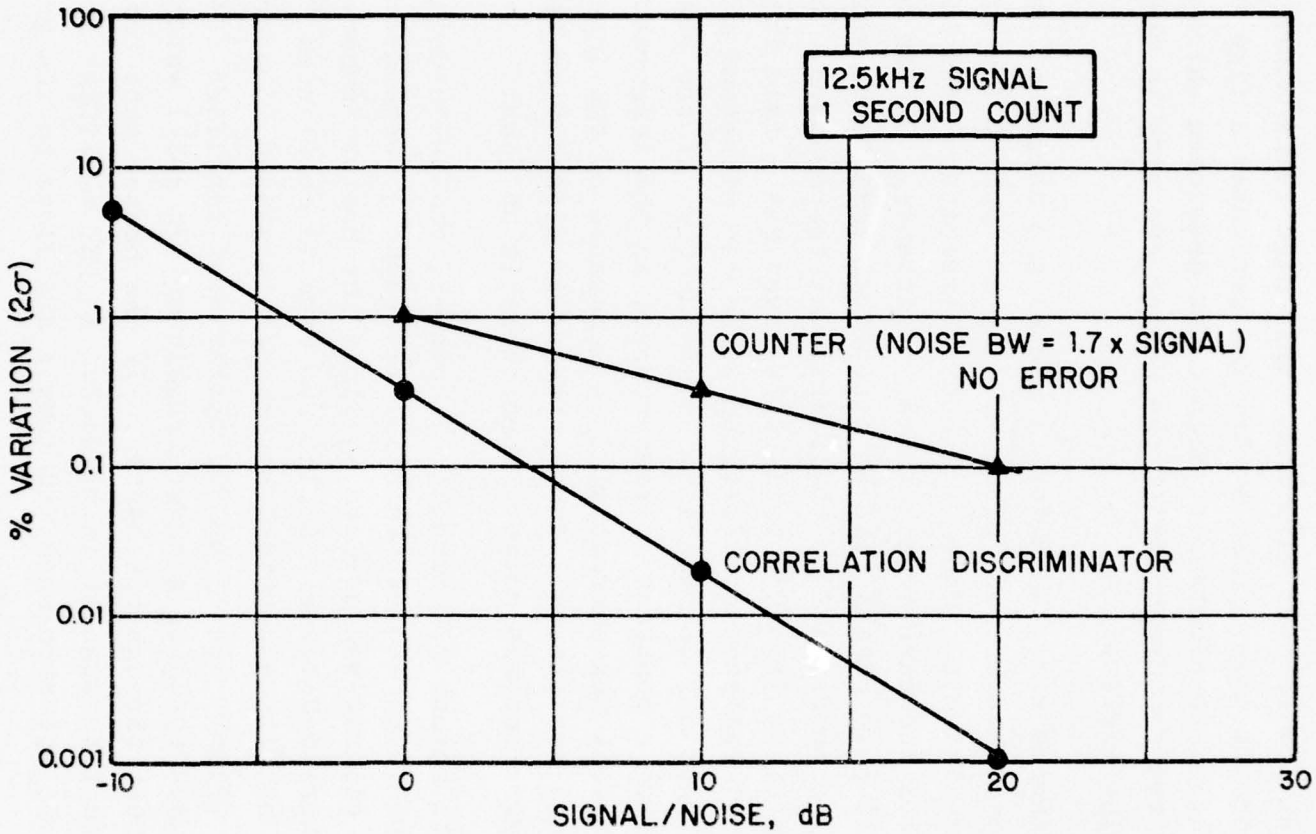

FIGURE 14. JITTER OF THE CORRELATION DISCRIMINATOR COMPARED WITH A COUNTER.

power dissipation from the wire was independent of the airflow over it. As a consequence, the wire became very hot and even glowed at low or zero airspeed. This high temperature tended to reduce the life of the heater and presented a fire risk. Accordingly, an electronic circuit was developed which limits the maximum temperature to which the heater can rise in the absence of cooling airflow.

Nichrome wire, an alloy of nickel and chromium, has a very small temperature coefficient of only 100 ppm/°C for its electrical resistance. Thus, a 1,000°C temperature rise will give only a 10% increase in electrical resistance. On the other hand, all pure metals have an electrical resistance which is directly proportional to their absolute temperature. A change in temperature from 0°C to 1,000°C gives a 4.7 fold increase in electrical resistance. Platinum wires can withstand this temperature without any degradation. Consequently, if the heater is driven from a constant voltage source, as the temperature of the heater rises, the current will fall because of the increase in electrical resistance. Hence, the power dissipation is reduced as the wire becomes hotter, when there is no flow.

This amount of protection, however, can be inadequate since high wire temperatures can still be reached; therefore, a heater control circuit was devised to limit the heater temperature to a predetermined value. A platinum wire is still used for the heater, but its electrical resistance is sensed in a bridge circuit (Figure 15) by an FET operational amplifier (CA 3031) and is used to drive a power transistor (2N 3024) which controls the current through the heater. If the heater gets too hot, the current through it is reduced. An FET amplifier is used because it operates when its inputs are close to the ground

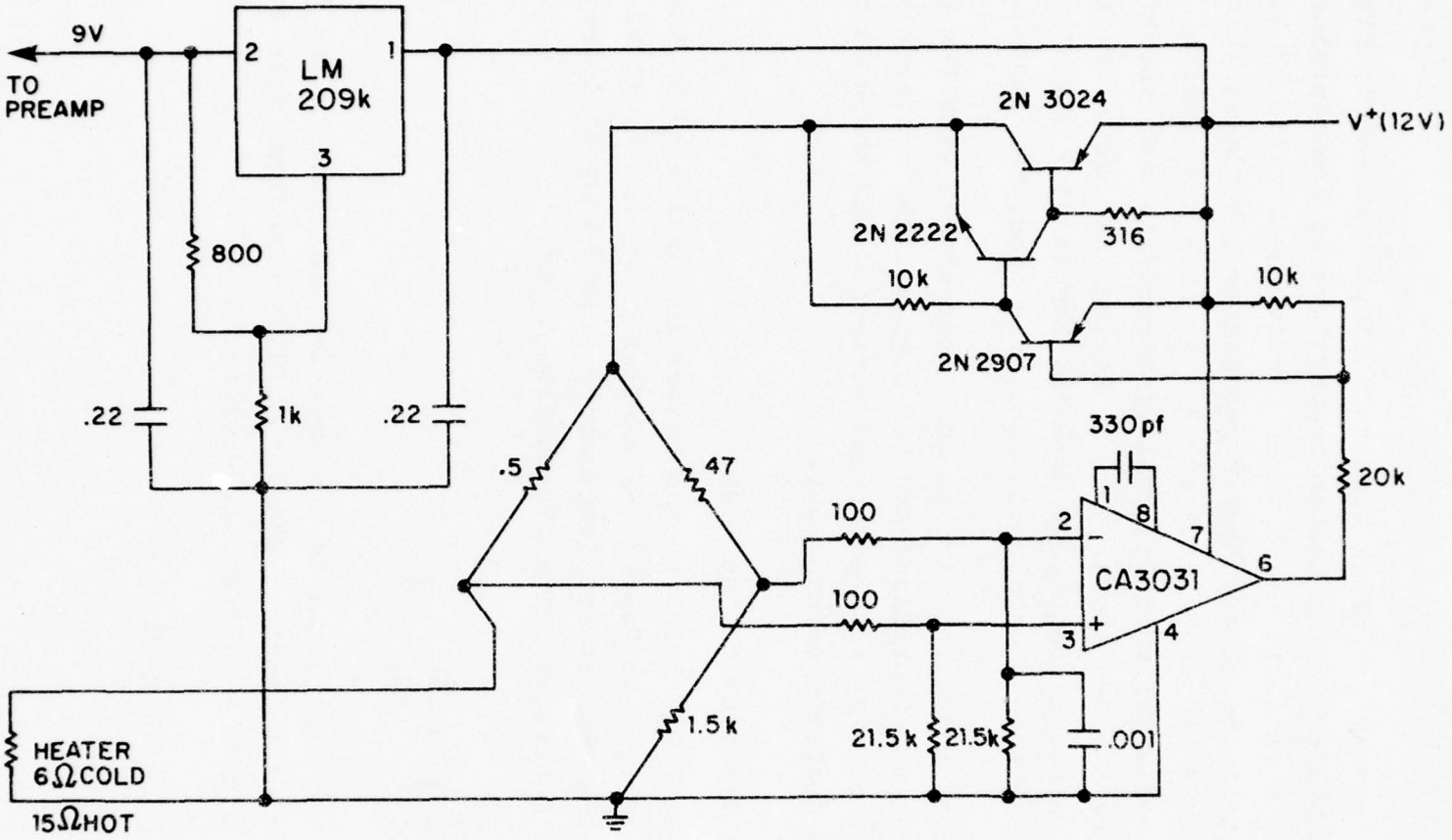

FIGURE 15. HEATER AND POWER SUPPLY REGULATOR CIRCUIT DIAGRAM

(which occurs at low airflow when very little current is flowing through the heater). The heater temperature is predetermined by the resistance ratio in the bridge. An overheat ratio of 2.5 was chosen to increase the heater resistance 2.5 times; this is equivalent to a temperature of 800°F. At this temperature, platinum's resistivity is 25% that of Nichrome's and, therefore, a heater wire 4 times longer, or one having half the diameter of Nichrome wire, is required. A 6-in. length of 2 mil diameter platinum wire, with a cold resistance of 6 ohms, was chosen.

This heater control circuit was incorporated with the power regulator for the photodiode and LED supply. The heater output is now substantially reduced at low airspeeds and there is no risk of the heater's burning out.

3.3.1 Heat transfer to the flow

The electrical input to the heater is dissipated in the hot wake which is used to "mark" the airflow. In Sec. 2, it was shown that the mean square temperature fluctuation $\overline{\theta^2}$ is related to the mean square velocity fluctuation $\overline{u^2}$ by

$$\left(\frac{\overline{\theta^2}}{\overline{u^2}}\right)^{\frac{1}{2}} = \frac{P}{FC_P} \quad ,$$

where P is the heat input to the wire per unit length, and F is the drag per unit length. Now for a fully turbulent wake at a distance x behind a cylinder of diameter d

$$u^2 \approx 0.1\, U^2\, \frac{d}{x} \quad ,$$

where U is the freestream velocity. Thus, for a fully developed turbulent wake

$$\overline{(\theta^2)}^{\frac{1}{2}} = \frac{0.31P}{1/2\rho\ C_D\ UC_P}\ \left(\frac{d}{x}\right)^{\frac{1}{2}} \quad .$$

Over most of the range of interest $C_D \approx 1$, $\rho = 1.2$ kg/m^3, and $C_P = 1.0$ joule/m^3/°k. Thus,

$$\overline{(\theta^2)}^{\frac{1}{2}} = 0.5\ \frac{P}{U}\ \left(\frac{d}{x}\right)^{\frac{1}{2}} \quad .$$

Typically, with x/d = 30, P = 100 watt/m, and U = 100 m/sec

$$(\theta^2)^{\frac{1}{2}} \approx 0.1°C \quad .$$

Goldstein* discusses the results of heat transfer by forced convection from a circular cylinder. His discussion is in terms of the Nusselt number which is defined by

$$Nu = \frac{P}{\pi \Delta T k} \quad ,$$

where K is the thermal conductivity of the fluid. Now,

$$Nu = \left(\frac{P}{\rho d U C_p \Delta T}\right)\left(\frac{d\rho U}{\mu}\right)\left(\frac{\mu C_p}{k}\right)$$

$$= \quad St \quad Re \quad P_r \quad ,$$

---

*S. Goldstein (ed.), 1965, *Modern Developments in Fluid Dynamics*, Dover Publications Inc., New York.

where Re is the Reynolds number, P_r is the Prandtl number, and μ is the dynamic viscosity. The Nusselt number varies with Reynolds number according to

$$Nu = C\ Re^{n} \quad ,$$

where C is a constant and the index n varies with Reynolds number, or

$$St = C\ Re^{n-1}\ P_r^{-1} \quad .$$

This relation has been found to hold well for gases where the Prandtl number is close to unity. (It is 0.74 for air at room temperature.) The results of an investigation by Hilpert* are shown in Figure 16. This investigation was performed for a cylinder at 100°C over a Reynolds number range from unity to 2.4×10^5.

Over the Reynolds number range of 250 to 10,000 which corresponds to the operating range of the OCV heater,

$$Nu = 0.5\ Re^{\frac{1}{2}}$$

or $$St = 0.675\ Re^{-\frac{1}{2}} \text{ for air} \quad .$$

Another form of this behavior is the well known King's Law for the hot wire anemometer where the power dissipation from the wire is proportional to the square root of the air velocity.

---

*Hilpert, 1933, Forsh. Ingwes 4, and 1932 Ver. Deutsch Ing. Forshungsheft., quoted in S. Goldstein, ibid.

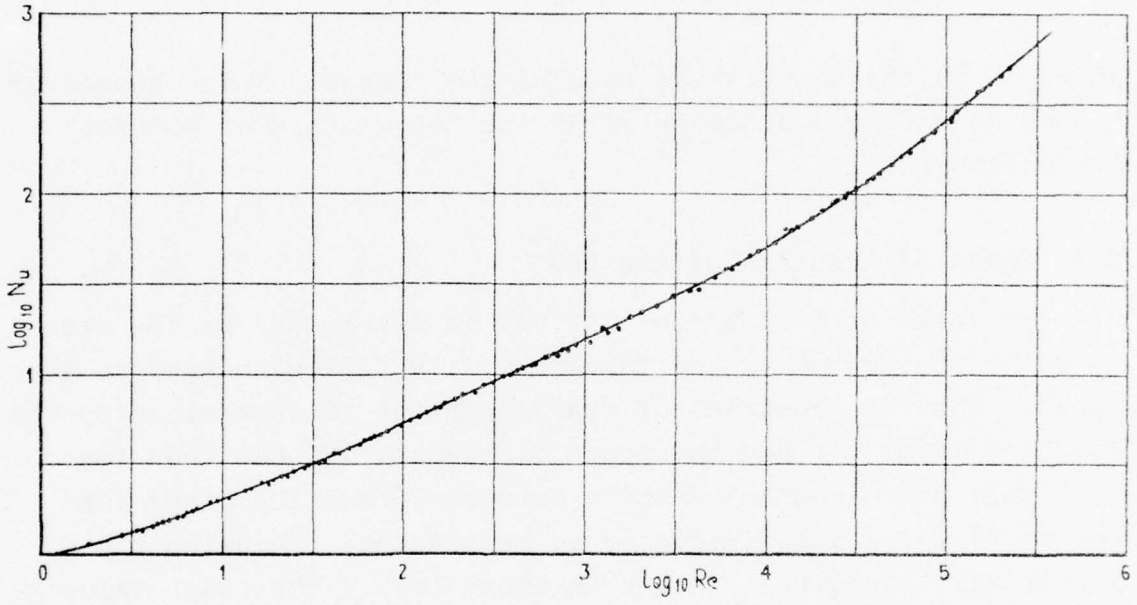

FIGURE 16. HEAT TRANSFER FROM A CIRCULAR CYLINDER.

The signal of the OCV is directly proportional to the rms temperature fluctuation in the heater wake. Thus, if we keep the power dissipation constant, as we do at high speeds, the signal strength is given by

$$\text{Signal} \propto P/U \quad .$$

However, at low speeds, the temperature of the heater is held constant by its protection circuit. Then,

$$\text{Signal} \propto \Delta T/U^{\frac{1}{2}} \quad ,$$

where ΔT is the temperature rise of the heater. This changeover occurs at a Reynolds number of 30 for 100 watts/m or 400 for 1,000 watts/m.

3.4 Speed of Response of the OCV

The speed of response of the OCV is determined by the rate at which the output of the integrator can follow changes to its input. The time constant of the integrator is determined by the feedback capacitor and the input impedance. It has been found that this time constant must be between 20 and 100 times the period of the lowest frequency to be tracked; otherwise the jitter will cause the circuit to loose lock. The exact value depends a little on the amplitude of the input signal. The value of the integrator constant was chosen to track a weak signal down to 1 kHz. This gave a time constant of 100 msec. However, if we are prepared to track only stronger signals down to 2.5 kHz (10 kts) then we may reduce the time constant to 10 msec.

Thus, the speed of response of the OCV is determined by the lowest velocity to be tracked, and a value of 100 msec has been chosen in the current design.

SECTION IV

ENVIRONMENTAL CONSIDERATIONS

To be a practical instrument, the OCV must be operational in a wide range of environmental conditions. It must be able to withstand temperature extremes, high altitudes, rain, vibration, and icing conditions. In addition, it must be corrosion resistant. This section will discuss these environmental factors and describe those which may present any particular problem. Special consideration will be given to operation in rain, the effects of fog and dust, and the practicality of deicing and anti-icing.

4.1 Low Pressure (0 to 48,000 ft)

Low pressures do not cause any special problems with the operation of the OCV. In fact, it has been shown in the previous study* that the sensitivity increases as the pressure decreases. The only potential problem is with the electronics. When the sensor returns to ground level, moist air can enter the optics chamber, which may produce condensation if the sensor is cooled. Condensation may degrade the optical properties of the system or produce electrical short circuits. This problem may be overcome using "O" ring seals to make the sensor head pressure-proof. The lens may be bonded into its mount with epoxy, and a pressure-proof connector must be used. The sensor body should be filled with dry nitrogen and some silica gel to keep it dry.

At high altitudes, where the density of the air is lower, the cooling capacity of air decreases. In addition, the electric breakdown field gradient is reduced and corona discharge is more likely. However, neither of these factors affect the OCV.

---

*M. Rudd (1975). "The Optical Convolution Airspeed Indicator," Technical Report AFFDL-TR-75-125, Air Force Wright Aeronautical Laboratories, Wright-Patterson Air Force Base.

4.2 Vibration

The OCV is somewhat sensitive to vibration. Vibration of the mirror/grating can cause the return image of the LED to move about on the photodiode, which will generate an output signal. However, if the mirror is mounted sturdily, this signal will be small. In addition, vibrations tend to occur at lower frequencies than those employed by the OCV. Typical vibration levels are 5g over a frequency range of 52 to 2000 Hz. The MIL-STD-810C curves are shown in Figures 17 and 18.

Electrical problems may arise from vibrating wires or other electrical components, but these can be controlled by conventional fabrication techniques.

4.3 Acoustical Noise

Acoustical noise can give rise to the same sort of problems as vibration. Generally, the displacements are smaller and the frequencies are higher. Again, a substantial mirror mount will solve these problems. Overall test levels should be (according to MIL-STD-810C) 160 dB for the sensor head and 140 dB for the power supply and processor. The spectrum is shown in Figure 19.

4.4 Rain

Rain can affect the OCV in two ways; (1) the raindrops passing through the measurement volume generate a signal and, (2) water on the lens and mirror degrades the performance of the optical system. Water cannot enter the body of the sensor since it is sealed with "O" rings to make it waterproof and pressure proof.

When a raindrop passes through the measuring region, it will actually enhance the signal and, as long as the raindrop

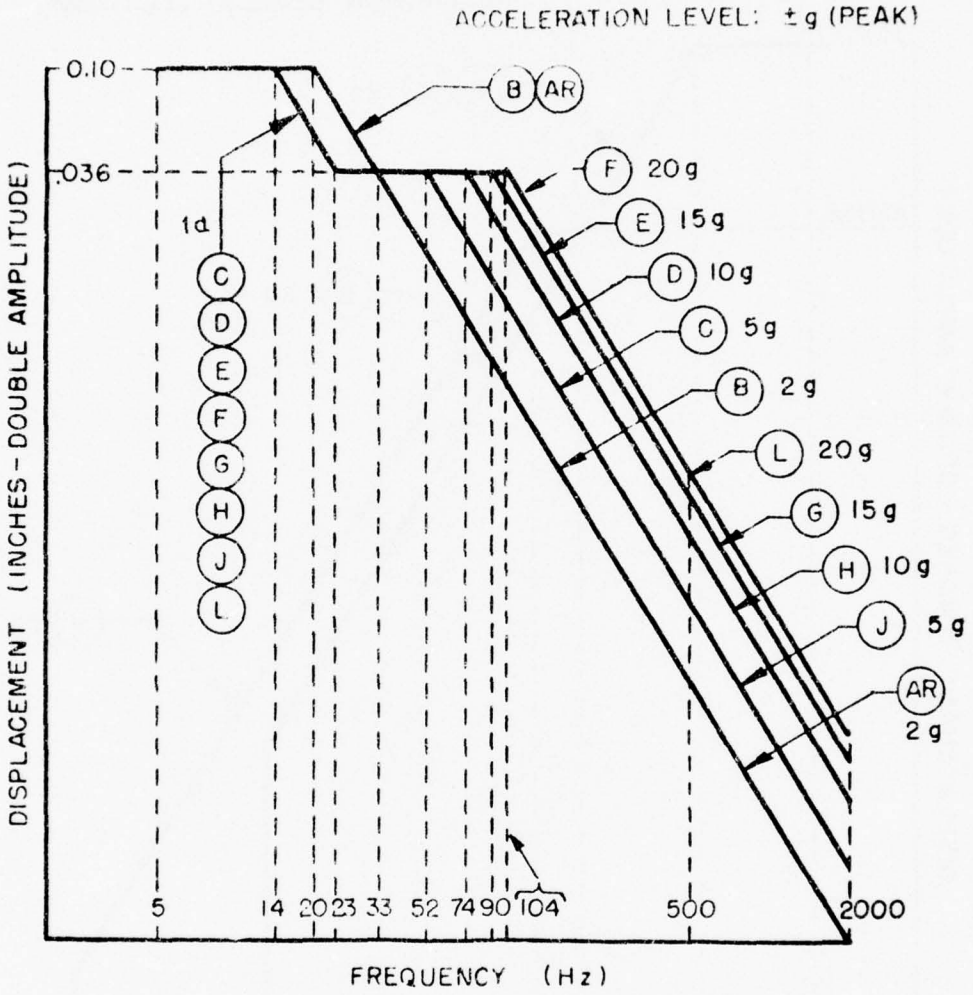

FIGURE 17. VIBRATION TEST CURVES FOR EQUIPMENT INSTALLED IN AIRPLANES, EXCLUDING HELICOPTERS, EQUIPMENT CATEGORY b.1. (MIL-STD-810C)

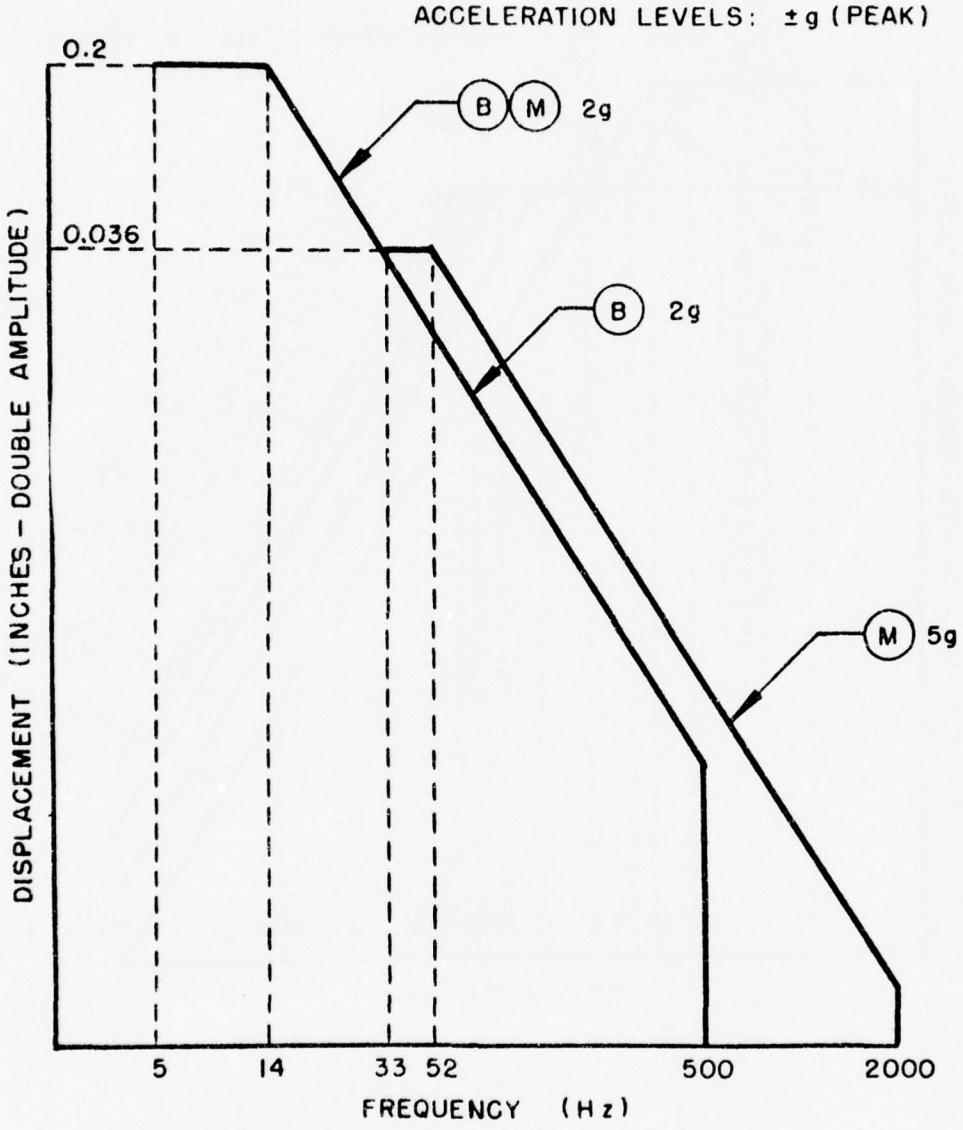

FIGURE 18. VIBRATION TEST CURVES FOR EQUIPMENT INSTALLED IN HELICOPTERS, EQUIPMENT CATEGORY c. (MIL-STD-810C)

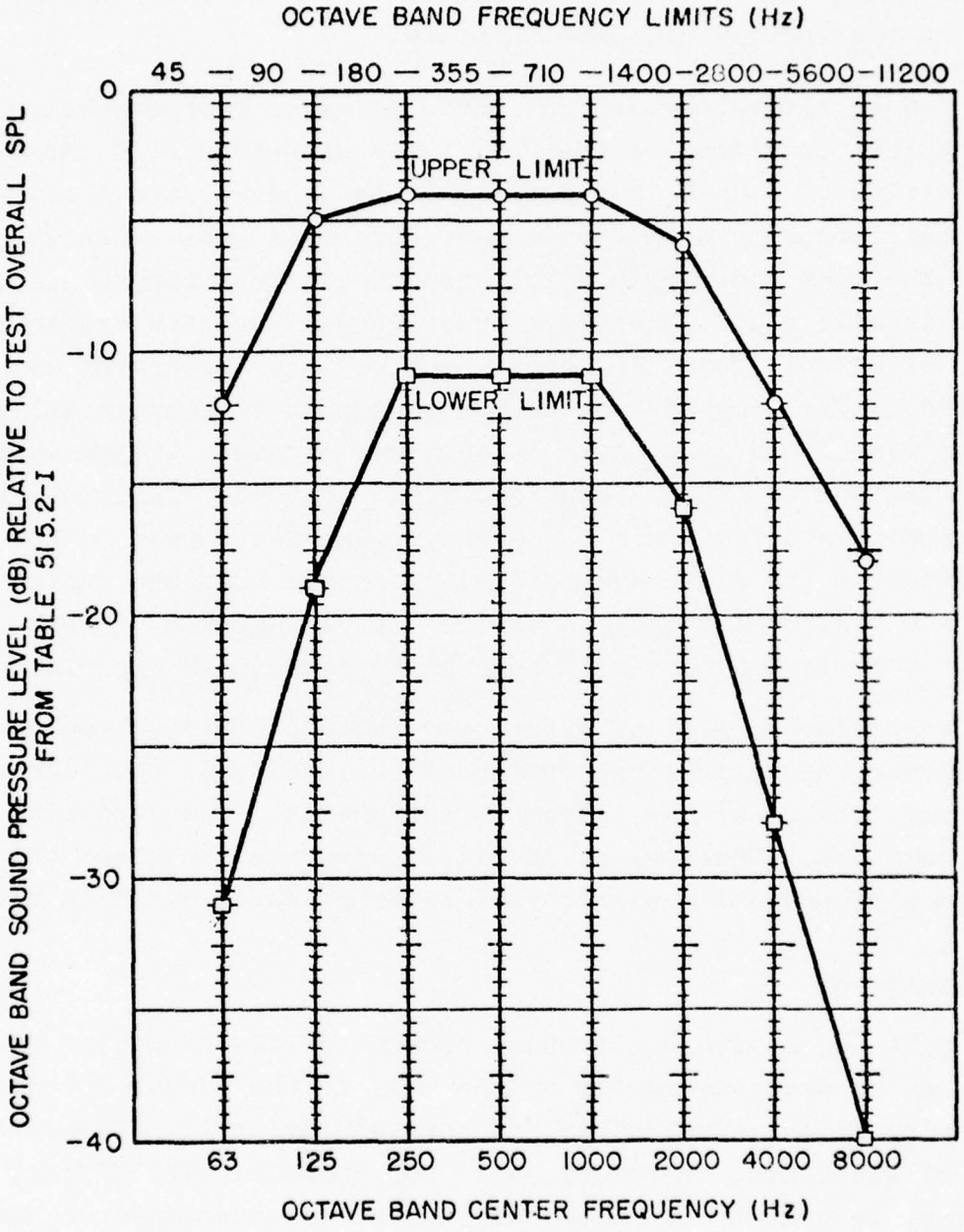

FIGURE 19. OCTAVE BAND SPECTRUM FOR THE ACOUSTICAL NOISE TEST. (MIL-STD-810C)

travels with the free stream airflow, will give a true reading of airflow. Errors may be introduced if the airflow is accelerating locally, for then a raindrop will lag behind the airflow. In these cases, the OCV will read closer to the free stream airspeed than to the locally disturbed airflow.

A more severe problem can occur if water droplets build up on the lens or mirror of the OCV. This situation will cause some degradation of signal, but worse, if the droplets are flowing, they can introduce a spurious low-frequency signal. However, since the lens and mirror are flush-mounted in their supports, droplets will only impact them under conditions of sideslip (or angle of attack, depending upon which way the instrument is mounted). The droplets on the surfaces move at substantially slower velocities than those in the free stream. It has been shown earlier that the signal processor tends to filter out low frequencies and lock onto the high frequencies caused by the raindrops in the flow. Therefore, we expect that the system will not "see" the raindrops on the optical surface. Whether or not this is the case will have to be determined experimentally.

A continuous film of water over the collimating lens or mirror can affect the optical properties of the system if the film is not uniform. The water may introduce astigmatism or defocussing of the radiation. However, it is likely, in practice, that the airstream will prevent a significant layer of water building up.

4.5 Salt Fog

Salt fog presents a problem because of its corrosive quality. This can be overcome as far as the body of the sensor is concerned by making it out of aluminum and hard-anodizing it. The lens is made of glass and, therefore, will not corrode. The mirror, however, is coated with aluminum, which is susceptible to corrosion. The aluminum is coated with a layer of silicon monoxide which renders it more durable; however, it is not yet certain that this coating is sufficient to prevent salt fog corrosion.

If further protection is desired, rhodium, which is completely impervious to corrosion, can be used instead of aluminum to form the mirror coating.

4.6 Dust

Dust cannot enter the sensor because the sensor is sealed; it can only settle on the optical surfaces and reduce the signal strength. However, this does not degrade the accuracy of the instrument since accuracy is determined by the frequency of the signal and not by its amplitude. The instrument will operate even with significant contamination of its surfaces. A 50% coverage of both optical surfaces will give a 9 dB reduction in signal.

Again, as with raindrops, dust in the airstream improves the signal rather than degrading it, because the instrument tracks the dust particles instead of the heater wake.

4.7 Humidity

Humidity does not affect the inside of the sensor because it is sealed. However, if high humidity causes condensation on the lens or mirror, the performance of the sensor will be impaired. This would probably not be a problem if it occurred in flight, since the slipstream would blow the condensation away; but. it could be a problem when the sensor is stationary on the ground. However, as we shall discuss shortly, the sensor head has to be heated for deicing purposes and this same heater can be used to remove condensation.

4.8 Fungus

Fungus can grow on any organic material such as paint. If the aluminum body of the sensor is anodized, however, and not

painted, fungus will not grow. If paint must be used, then a fungicide can be incorporated to prevent fungus growth.

4.9 High Temperature (71°C Maximum)

Although high temperatures can cause failure of electronic components and degradation of rubber and plastic components, components are readily available which can withstand these temperatures. Generally, CMOS circuits in plastic packages will withstand 85°C and those in ceramic hermetic packages will withstand 125°C. The LED must generally be derated to withstand 71°C for a long period. A maximum current of 75 ma is fairly typical. The photodiode is specified for a maximum temperature of 80°C. The other optical components can also handle 71°C with no difficulty.

4.10 Low Temperature (-55°C Minimum)

Low temperatures can also generate problems, primarily from differential expansion; in addition, components can become brittle. Therefore, it is most important to use electronic components having the correct temperature range specification. Regular CMOS circuits in plastic packages operate over a temperature range of -40°C to +85°C. However, circuits in ceramic hermetic packages will operate over a temperature range of -55°C to +125°C, and should be used when temperatures below -40°C are anticipated. Of the LEDs discussed, only the SSL 55c is specified for use down to -65°C. The other LEDs can only be used down to -40°C. Photodiodes are also available which can operate down to -55°C, although their sensitivity is somewhat reduced at this temperature.

4.11 Electromagnetic Interference (EMI)

Electromagnetic interference may produce spurious signals which can give an erroneous reading. The correlation discriminator, which contains an integrator, is not sensitive to one-time switching transients or pulses. However, it will be sensitive to continuous signals in the range of 1 to 100 kHz. The photodiode used as a radiation detector is very sensitive to electromagnetic interference, as has been found with fiber optic systems. In fact, the photodiode is sensitive to an induced current of only 2 nanoamps. Further, since it is a diode, it will rectify radio frequency transmissions and present the audio component to the amplifiers. Accordingly, it is very important that the photodiode be well shielded from all electromagnetic fields.

This shielding is accomplished by the aluminum housing of the sensor which is electrically connected to the same ground as the photodiode and preamplifier. Precautions must be taken when the aluminum is anodized since this makes the surface insulating and can prevent electrical connection between parts of the housing. The only unshielded area around the photodiode is the glass lens, which is inherently an insulator. However, this lens is 3-1/2 inches away from the photodiode and the absence of shielding may not be important. If tests should prove otherwise, the lens can be coated with a transparent electrode, such as tin oxide, that can be connected to the case. The photodiode would then be completely shielded.

Care must be taken in grounding the sensor case. If the power supply is not grounded (floating) then the case may be connected to the airframe. However, if the power supply is grounded, then the sensor must be insulated from the airframe.

Otherwise, if the system is grounded in two places, a ground-loop is developed and the system becomes extremely sensitive to electromagnetic interference.

The power supply line may be another cause of troublesome interference. Any ripple here is amplified by the photdiode preamplifier. The best way of eliminating this effect is by incorporating a three-terminal power supply regulator for the sensor. This has been very successful in eliminating 60 Hz and 400 Hz ripple from the system.

The OCV should be qualified in accordance with MIL-STD-461A, Class ID.

4.12 Deicing and Anti-icing

It is essential that the OCV sensor operate in all weather conditions, including freezing rain and crystallizing ice. The sensor must be capable of both removing ice which has built up on it while the aircraft was parked (deicing) and preventing ice buildup in flight (anti-icing). A typical specification calls for the instrument to be set up in an icing wind tunnel at an indicated airspeed of 350 kt ±25 and a temperature of -30°C ±5. Water droplets are sprayed into the airflow at a density of 1.25 grams ±0.25 per cubic meter. Ice is allowed to build up on the instrument; the heater is then turned on and must remove the accumulated ice within 1-1/2 minutes and keep the instrument free of ice.

The OCV is probably much less sensitive to icing than the Pitot-static tube since it does not have small holes which can clog with ice. However, a buildup of 1/4-in. of ice around the

sensor will cause a change in the aerodynamic flow which in turn can give an erroneous reading. Accordingly, some deicing and anti-icing precautions must be taken.

Heat must be applied to the sensor head to raise its surface about 0°C in a 350 kt airstream at a temperature of -30°C. However, not all exposed surfaces require heating; the water droplets will tend to impact on the leading surfaces and not on the trailing surfaces. A typical leading edge requires a heat density of 20 watts/sq in. and the area behind needs only 10 watts/sq in., while the trailing edge requires none. The tip of a Pitot tube requires only 40 watts/sq in. In the present design, the OCV has a rectangular flow tube 3 × 2 × 3.5 inches long. Let us suppose that it is sufficient to heat the front 1 inch of this tube with a power density of 15 watts/sq in. The remainder of the tube and optical surfaces would be heated by conduction, and in addition, very little ice would build up on them. Thus, for the 19 sq in. of exposed surface, 285 watts of heating power would be required. A sketch of the deicing heater is shown in Figure 20.

This 285 watt heater should be run off 28V dc since a 115V/400 Hz supply would generate a great deal of electromagnetic interference which would be detected by the photodiode.

If the heater is turned on when there is no airflow to cool it, it will become very hot. However, there are no heat sensitive components in that part of the sensor (the electronics are located farther down in its body). The mirror, lens, and aluminum body can all withstand temperatures of several hundred degrees. The most sensitive item is the "O" ring used to seal the lens into the body; however, there are other seals available which can withstand these conditions.

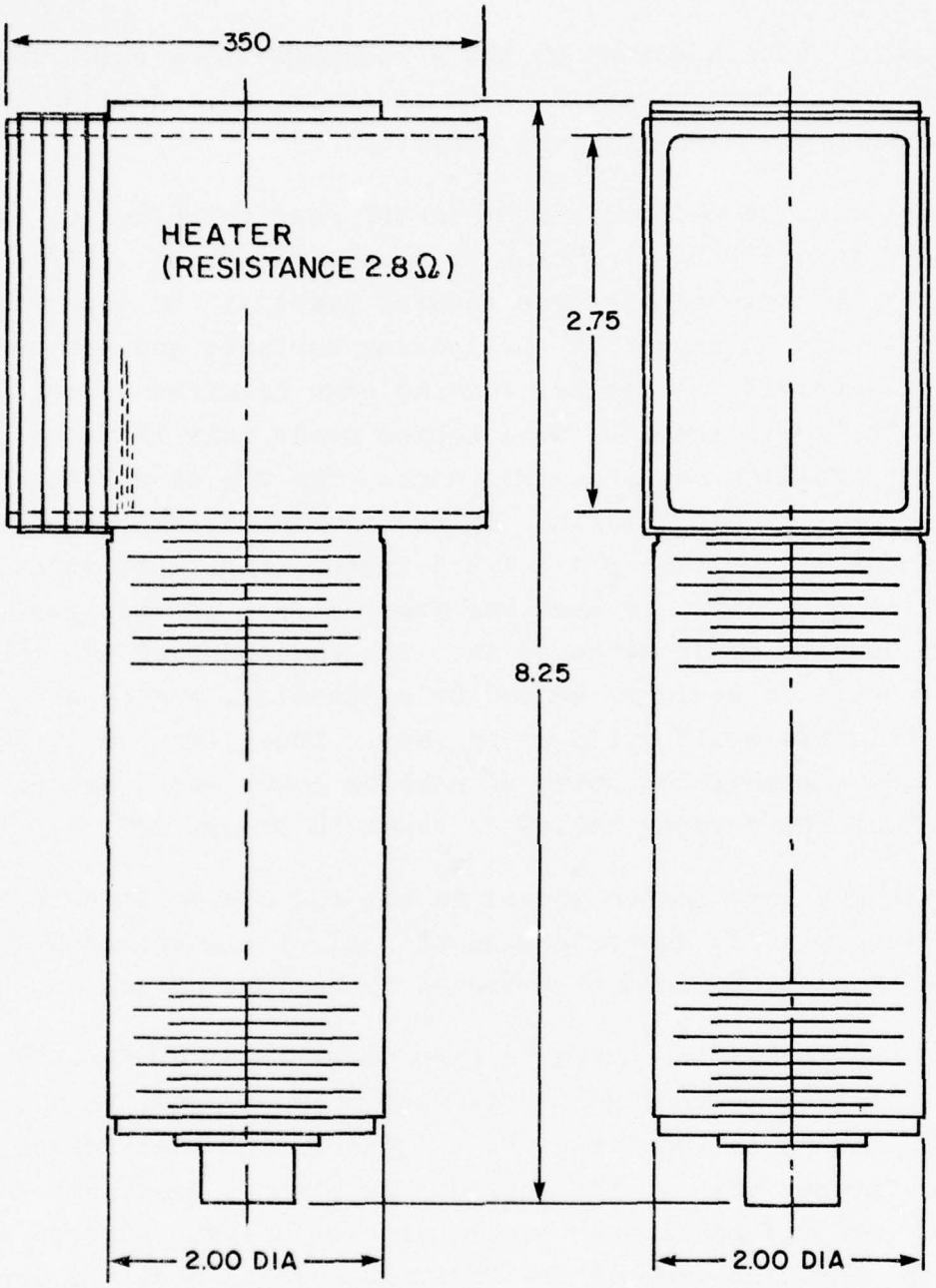

FIGURE 20. DEICING/ANTI-ICING HEATER ON OCV.

4.13 Installation and Operation on an Aircraft

4.13.1 Power supply requirements

The OCV has its own power supply in order to minimize electromagnetic interference effects and, thus, the choice of aircraft supply can be quite flexible. The OCV itself operates on 10 to 15 volts dc; its power supply can be designed to operate from either 28V dc or 115V ac. The deicing heater must operate from 28V dc, however, or the electromagnetic interference will be excessive. Operation from a 28V dc supply is easier and simpler since no transformer, rectifier, or smoothing is required.

4.13.2 Physical location on aircraft

Ideally, the OCV should be mounted at some position on the aircraft where the airflow is undisturbed. Unfortunately, such a position does not exist on an aircraft. It is fairly easy to mount the sensor head outside the aircraft's boundary layer which is only a fraction of an inch thick at the front. However, it is virtually impossible to mount the sensor outside the potential flow disturbance around the aircraft. This disturbance is produced by the air flowing around the aircraft and is typically 10 to 20% of the free stream velocity. This disturbance is a function of position on the aircraft, Mach number, angle of attack, and sideslip. Pitot tubes are usually mounted on the fuselage near the nose, which makes the pressure lines to the air data computer short. The OCV could be mounted on the wings where the flow is relatively unaffected by sideslip but there it would be affected by angle of attack, flaps inboard, and ailerons outboard.

In practice, the airspeed system of an aircraft is "calibrated." That is, its dependence on Mach number, angle of attack,

sideslip, and external configuration is determined empirically and this information is stored in an air data computer. Once in flight, all of the airspeed measurements are corrected for these factors. It is difficult to see how this can be avoided with the OCV unless it is mounted well away from the aircraft.

It is important that the airflow around the region where the OCV is mounted be reproducible. The OCV should not be mounted close to flaps, undercarriage, control surfaces, or engines. The nose of the aircraft or the top of its tail would be good positions at which to mount the OCV. However, reading from both of these positions will have to be corrected for airframe disturbance effects.

4.13.3 Output data format

There are a host of different formats by which digital instruments can communicate with one another. They generally use a code called Binary Coded Decimal (BCD) in which the numbers 0 to 9 are represented by a binary code of 4 bits. Thus, an output of 4 digits would be represented by 16 bits in 4 groups of 4. These bits may be in parallel (this requires at least 16 wires) or in series (on one wire). Although the latter is generally preferred because it needs less wiring, it is much more complicated. The beginning and end of the series of bits have to be identified, the transmitter and receiver synchronized, and the transmission rate standardized.

MIL-STD-1553A lays down a format for such a system. In addition, ARINC has two standards for data transmission. It is, however, a fairly involved process to translate the digital data into the required format and would add substantially to the cost of the OCV.

In order to maximize system flexibility in light of these various standards, it is recommended that the output of the OCV be the VCO output, which is a square wave with frequency directly proportional to airspeed. This frequency can be used to drive a cockpit display or an air data computer. TTL logic levels are most commonly used and, therefore, a square wave between 0 and +5V is most appropriate.

4.14 Conclusions

There are no environmental conditions under which the OCV can not operate. The proper choice of components will protect against temperature extremes and corrosion. Dust does not present a problem unless a very heavy buildup occurs, in which case the OCV can be cleaned. The problem of electromagnetic interference is solved by shielding the sensor, providing it with its own stabilized power supply, and grounding it properly. Deicing and anti-icing are accomplished by installing a heater on the sensor head. The OCV is not as sensitive to icing as a Pitot tube is, since it can operate with some buildup on it. Vibration, acoustical noise, and rain are not expected to present any problems, although tests should be performed to verify this.

The OCV operates best from a 28V dc aircraft power supply, although a 115V 400 Hz supply with a converter could also be used. The OCV is best mounted on the aircraft nose or tail but there will always be flow disturbances generated by the aircraft for which the OCV must be corrected. The most flexible OCV output format is the VCO output which is a square wave of a frequency directly proportional to true airspeed.

SECTION V

TESTING AND EVALUATION OF THE OCV

5.1 Wind Tunnel Testing

The OCV Prototype MKII was set up in the BBN free jet wind tunnel. This tunnel has a working section 4 ft in diameter and is capable of operating over a speed range of 30 to 300 ft/sec. It is powered by a 600-Hp diesel engine. The tunnel speed is measured by a transducer which measures the difference in static pressure across the tunnel nozzle. The signal is linearized, compensated for ambient temperature (but not barometric pressure), and displayed on a digital panel meter. The calibration of the speed indicator is shown in Figure 21. The calibration was performed against a water manometer at a temperature of 80°F. The speed indicator read correctly at 25 mph but underindicated by 2 mph at 50 mph.

5.1.1 Heater output

The OCV heater was designed to give a 25-watt output in a moderate airflow and yet limit the heater wire temperature to 800°F when there was no cooling airflow. Accordingly, the heater power output was measured as a function of airspeed and the results are shown in Figure 22. The output was much less than expected, reaching 6.5 watts at 120 mph. It is thought that the reason for the low power output is that a coil wound on an insulating rod cannot dissipate heat as efficiently as a continuously coated rod. A continuous platinum film instead of a wound wire should be considered as an alternative in fabricating the heater.

Because of the low heat output, the OCV could not be operated at high speeds. In fact, satisfactory operation could not be obtained above a speed of approximately 55 kts.

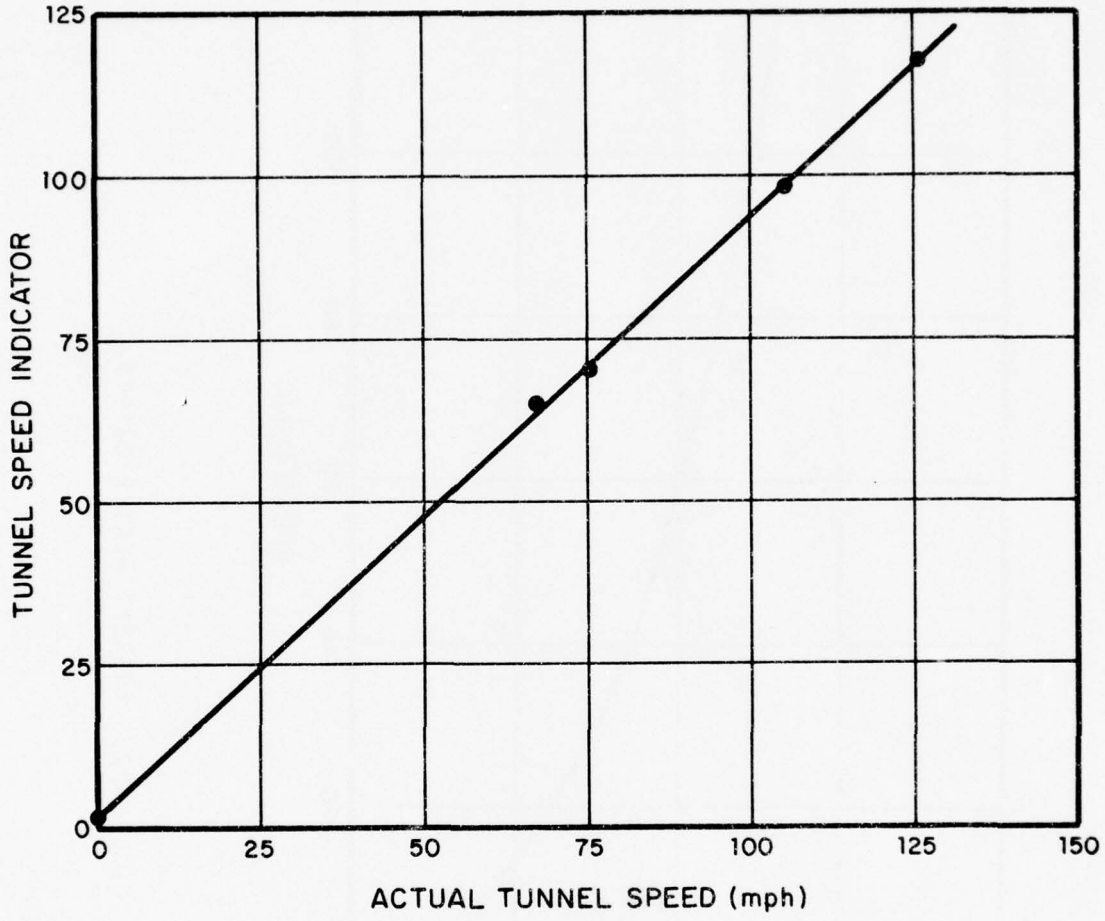

FIGURE 21. CALIBRATION OF WIND TUNNEL.

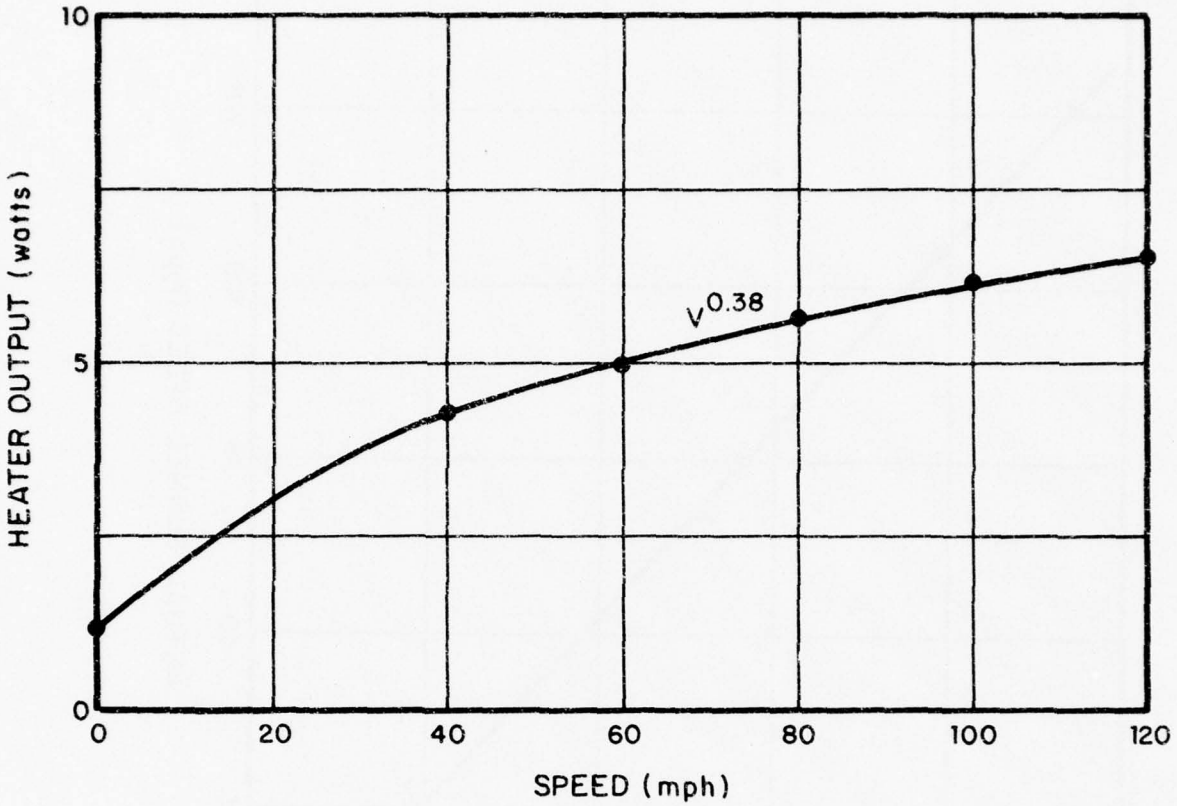

FIGURE 22. PRESENT HEATER OUTPUT.

5.1.2 Flow tube configuration

Three configurations of the OCV were tested in the wind tunnel. The first of these was the "flow tube" configuration in which the measuring region was surrounded by a rectangular tube 2 x 3 x 3 1/2 in. long. The ends of the tube were beveled to improve flow characteristics. The performance of the OCV as a function of its angle of attack (α) and sideslip (β) were investigated. These two angles are interchangeable, but we arbitrarily decided to define the optical axis vertically. Sideslip then corresponded to rotation about the optical axis.

The result can be seen in Figures 23 and 24. Large increases in readings are seen for angles of attack greater than $+10^{\circ}$; readings could not be obtained at large negative angles of attack and high speeds because of the high turbulence levels resulting from separation in the flow tube. The response to sideslip in Figure 23 is close to $(\cos \beta)^{-1}$ with an offset of about 3°.

5.1.3 Open cage configuration

In this configuration, the mirror grating was supported on four slender posts, leaving the measuring region as open as possible. The performance as a function of angle of attack (α) and sideslip (β) are shown in Figures 25 and 26. The OCV reading dropped about 7% for an angle of attack of $\pm 10^{\circ}$ and was then fairly constant for higher angles. The response to sideslip was approximately proportional to cos β, except at high positive angles where the discrepancy cannot be explained.

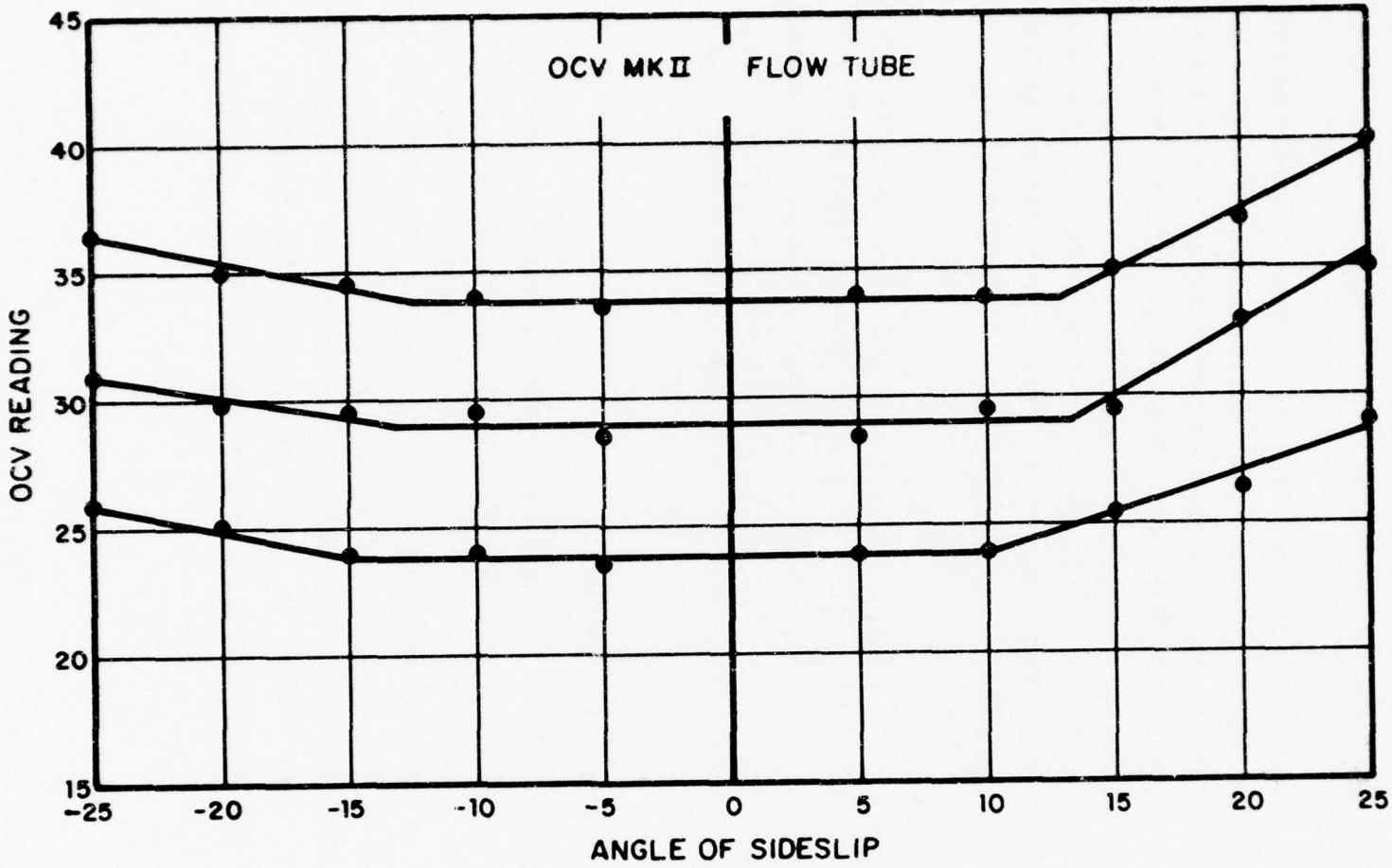

FIGURE 23. RESPONSE OF OCV TO SIDESLIP (FLOW TUBE CONFIGURATION)

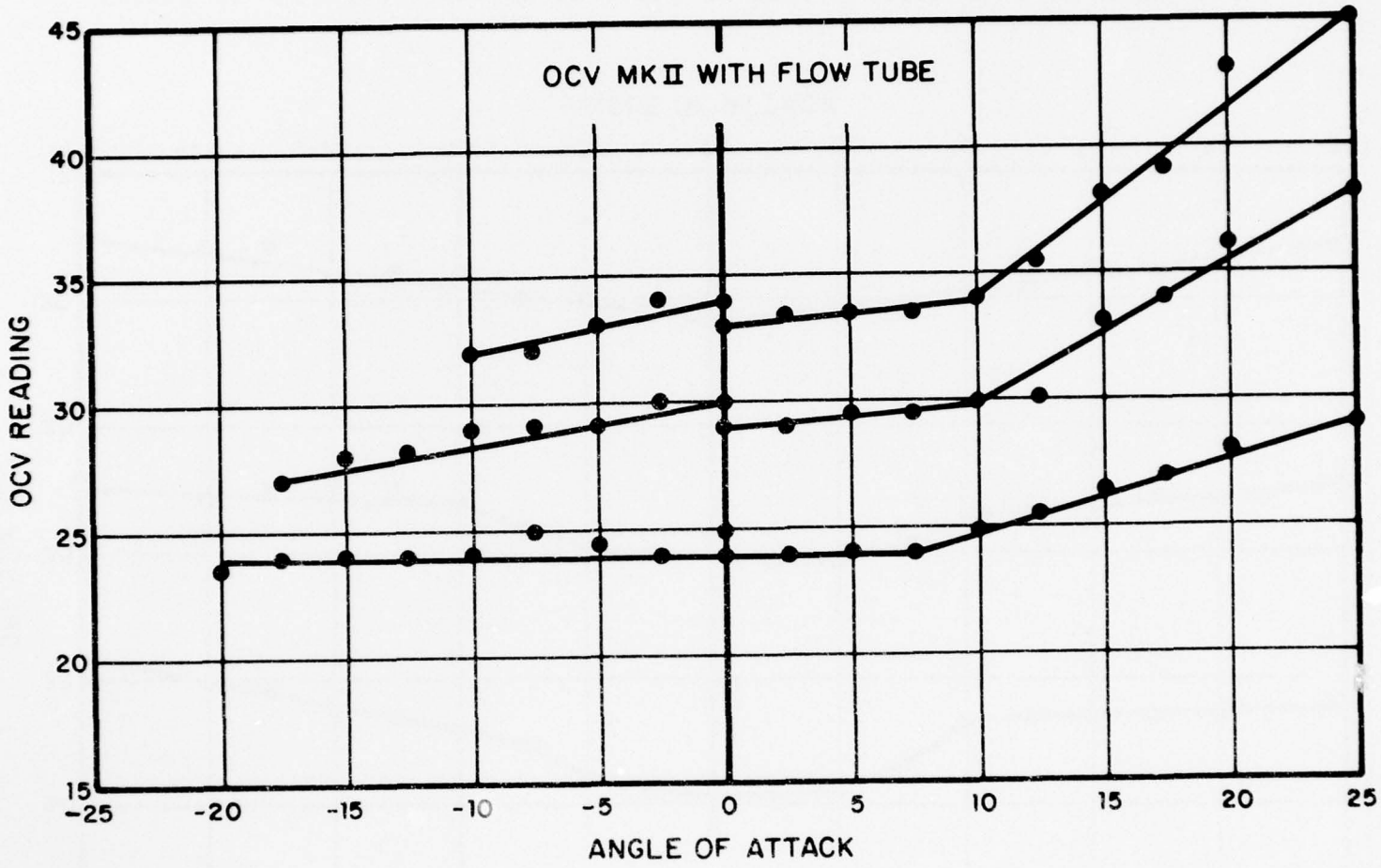

FIGURE 24. RESPONSE OF OCV TO ANGLE OF ATTACK (FLOW TUBE CONFIGURATION)

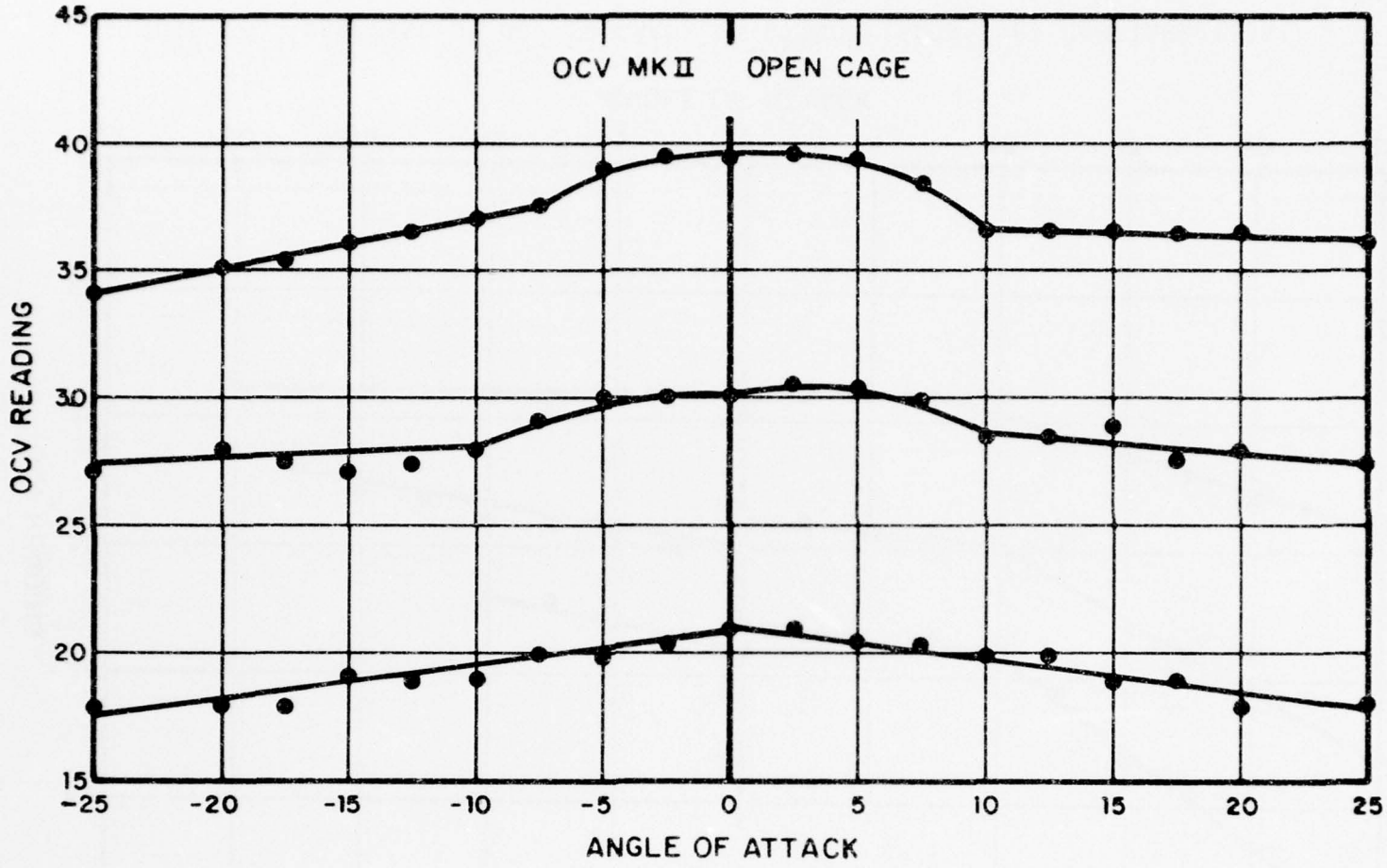

FIGURE 25. RESPONSE OF OCV TO ANGLE OF ATTACK (OPEN CAGE CONFIGURATION)

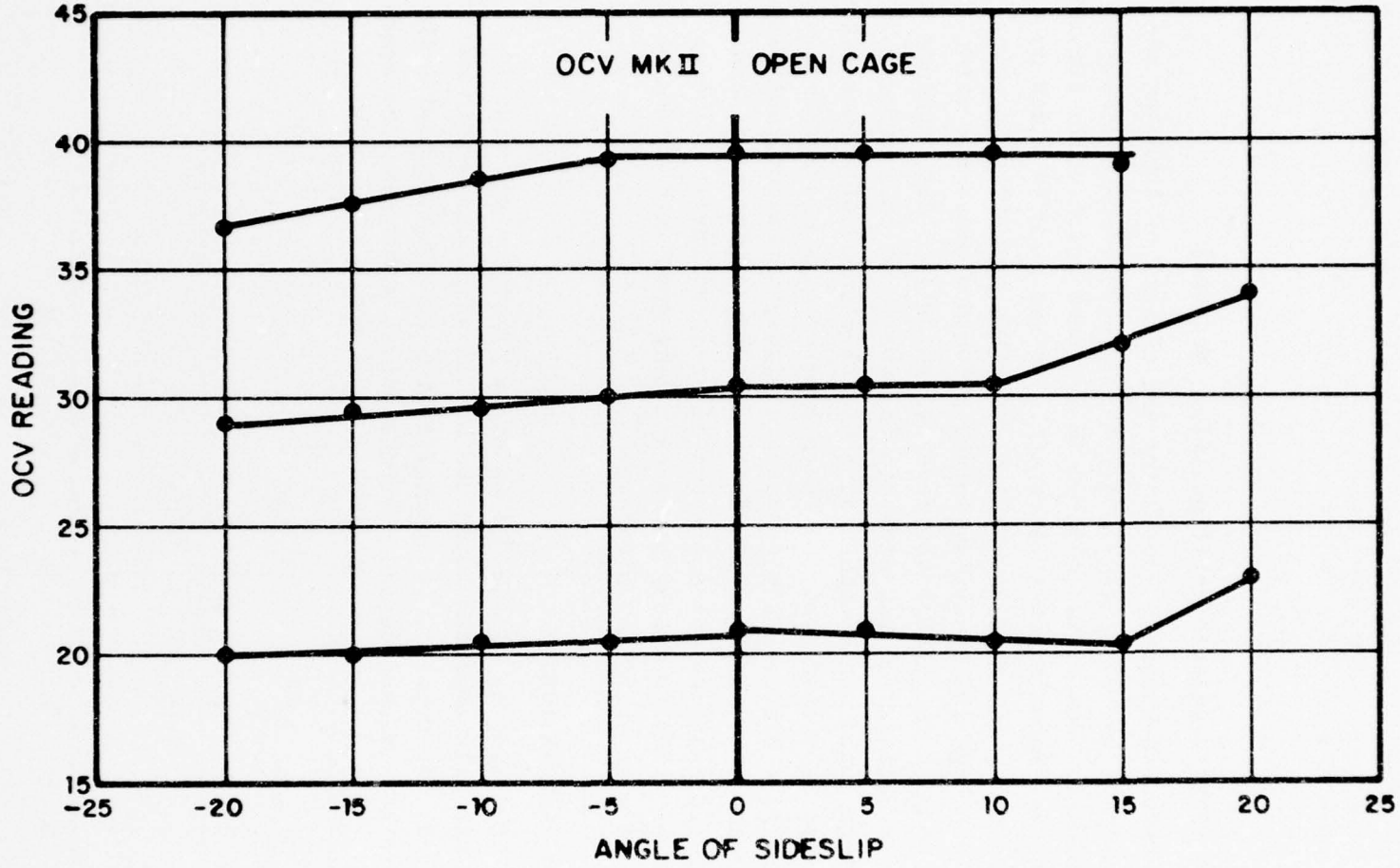

FIGURE 26. RESPONSE OF OCV TO SIDESLIP (OPEN CAGE CONFIGURATION)

5.1.4 Open cage configuration (flush mounted)

Next, we wanted to determine the effects of changing the mounting of the OCV. Previously it had been supported bare in the tunnel. Now it was mounted in a manner which would simulate the actual mounting on an aircraft. It was mounted flush on a square plate (18 x 18 in.) which simulated the aircraft skin. Only the cage and measuring volume protruded above the skin; the main body of the sensor was recessed below it. The response to angle of attack (α) and sideslip (β) are shown in Figures 27 and 28. Readings could not be taken at a positive angle of attack because the flow separated from the sharp leading edge of the 18-in. square flat plate. This produced a highly turbulent, unsteady flow in the measuring region. At negative angles of attack, the change in response was approximately proportional to sine α. The angle of sideslip response was extremely good with errors of less than 4% even at 20° of sideslip.

5.1.5 Conclusions

The response of the OCV to angle of attack and sideslip is very strongly dependent upon the way in which the sensor head is mounted. At present, it appears that a configuration with the sensor head flush mounted on the aircraft skin gives the best performance

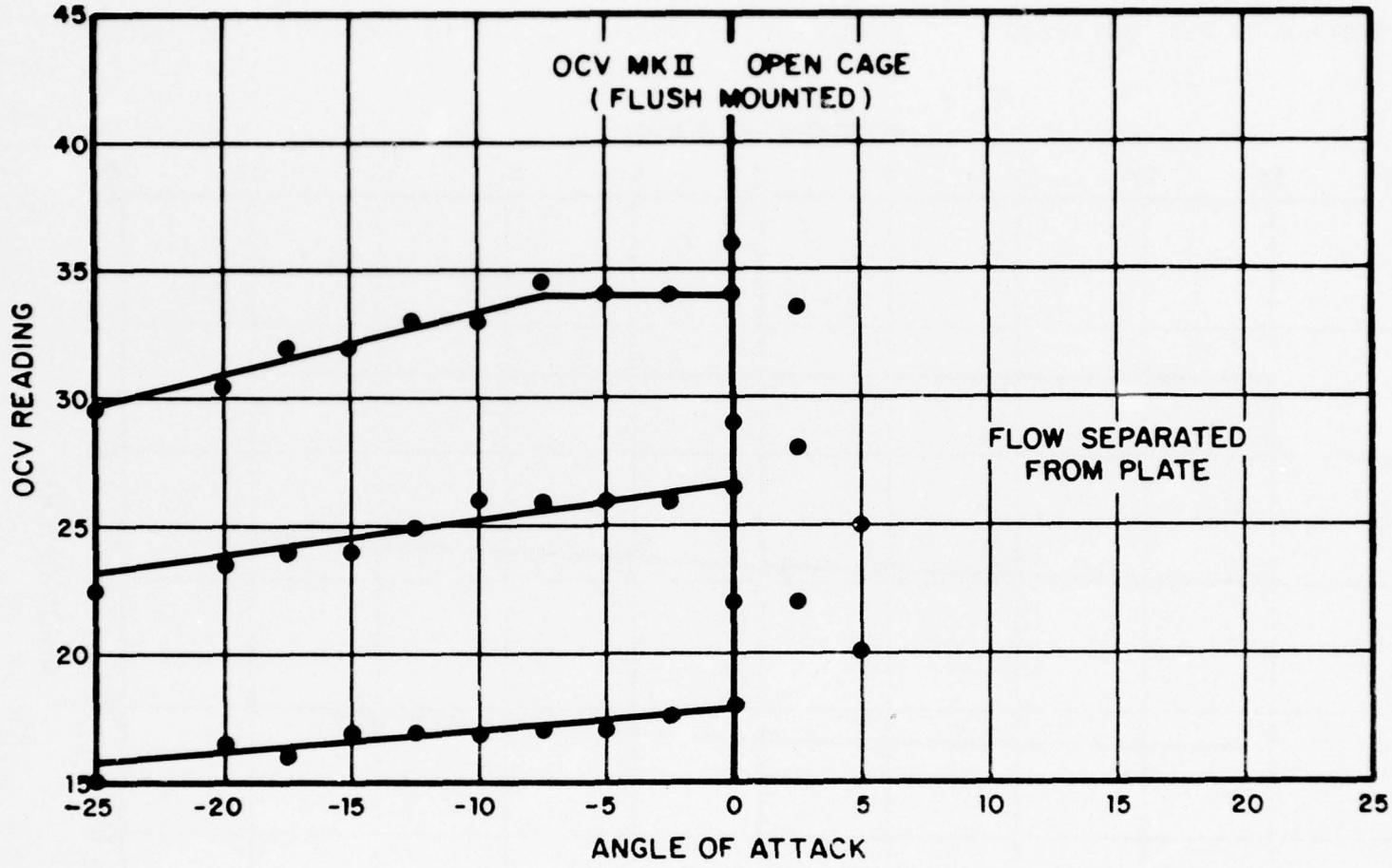

FIGURE 27. RESPONSE OF OCV TO ANGLE OF ATTACK (OPEN CAGE CONFIGURATION, FLUSH MOUNTED)

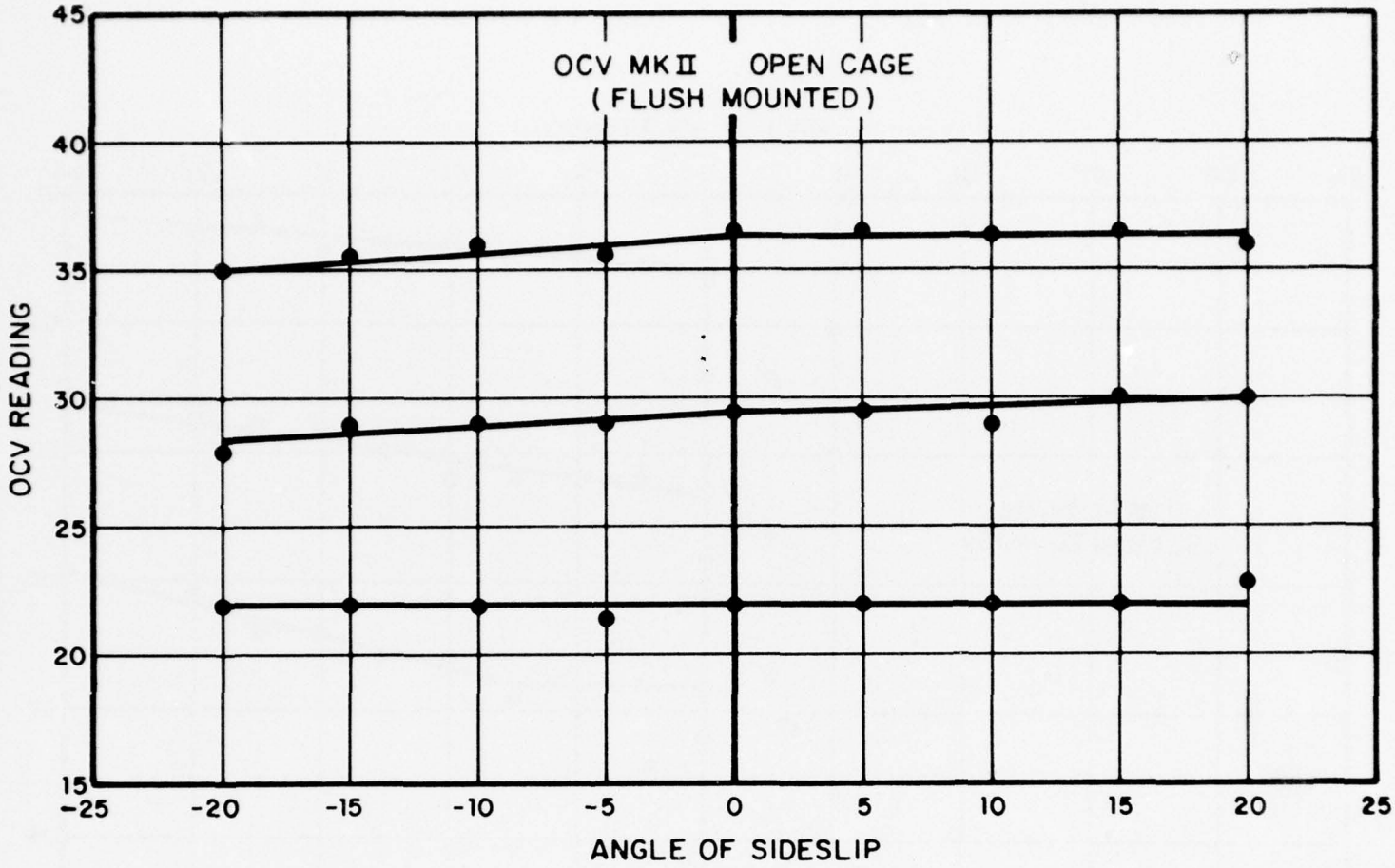

FIGURE 28. RESPONSE OF OCV TO SIDESLIP (OPEN CAGE CONFIGURATION, FLUSH MOUNTED)

SECTION VI

RECOMMENDATIONS FOR FURTHER WORK

This program for the development of the Optical Convolution Airspeed Indicator is now at the stage where the prototype unit works well in the wind tunnel. The next stage in the development program will be to demonstrate the operation of the instrument under realistic environmental conditions. This will require environmental testing of the unit for temperature, vibration, shock, low pressure, humidity, salt fog, and electromagnetic interference.

It will also be necessary to provide the unit with the capability of operating under icing conditions. To do this, a deicing/anti-icing heater must be designed, developed and tested, following the recommendations made in Section 4 of this report.

The aerodynamic performance of the OCV under angle of attack and sideslip still leaves something to be desired. Improvements such as a cylindrical flow tube instead of a rectangular one should be considered.

When these features have been incorporated in the OCV design, it can be thoroughly tested and qualified for flight. Then the unit can be mounted on an aircraft and extensively evaluated over a long period of time.

SECTION VII

CONCLUSIONS

A second version of the Optical Convolution Airspeed Indicator has been built and successfully operated as a complete system. A substantial improvement in the signal-to-noise ratio has been effected by choosing a heater diameter of 30 mils, which is well matched to the grating pitch of 80 mils. An original technique for signal processing that is capable of measuring the frequency of a signal buried in noise has been invented. This circuit has greatly enhanced the performance of the instrument.

The environmental conditions under which the OCV will have to operate have been considered and no particular problems have been found. Appropriate components must be selected to operate over the temperature range required and the right materials must be chosen to avoid corrosion. The sensor head should be made waterproof and pressure proof. The detector must be well shielded against EMI, and the power supply must be well regulated.

A redesigned sensor has been built (complete with output display) and tested in a wind tunnel. The performance as a function of angle of attack and sideslip was investigated. Substantial variations were found as a result of changes in airflow around the sensor. Further aerodynamic investigations should be undertaken to minimize these variations.

APPENDIX

COMPARISON OF LIGHT EMITTING DIODES, TUNGSTEN FILAMENT LAMPS, AND LOW AND HIGH PRESSURE DISCHARGE LAMPS

1. Tungsten Filament Lamps

In the earlier study, only light emitting diodes (LEDs) were considered as radiation sources for the OCV. Infrared diodes were found to be the most efficient with some inexpensive devices emitting 5 mwatt of radiation for a driving current of 100 mamp at 1.5 volts. However, this voltage matches poorly the 12 volts for which the instrument was designed and, therefore, conventional tungsten filament lamps were considered.

There are some basic differences between tungsten filament lamps and LEDs. The latter produce a narrow spectrum about 40 nm wide, centered at 940 nm in the near infrared. Tungsten lamps produce a very wide spectrum from 400 nm to 3,000 nm with a peak at about 1,000 nm. Further, the light output from a tungsten lamp is nearly omnidirectional. Since the output has such a broad spectrum, it is rated in terms of visual brightness or candlepower. The relationship between candlepower and milliwatts of light (in which LEDs are rated) is a function of the color temperature of the lamp. However, the manufacturer of the photodiode has quoted both sensitivities of the detector as follows:

Sensitivity = 0.6 ma/mw at 900 nm
= 8.5 ma/lumen at a color temperature of 2850°k.

These values depend on the spectrum of the source employed, but they are, in fact, very close to the spectra of infrared LEDs and tungsten lamps.

Table 1 compares the relative photocurrents to be expected from three LEDs, five conventional tungsten filament lamps, and five halogen cycle lamps. For comparison purposes, the output of the lamps is assumed to be collimated by f/3 optics. This will

TABLE 2

COMPARISON OF SOURCES FOR OCV

Source No.	Type	Diameter (inches)	Output	Voltage V	Current ma	Collimated[+] Output	Relative* Photocurrent
SG1009A	LED	0.2	7.0 mw	10.5	100 ma	2.1 mw	1.2
TIL 31	LED	0.2	6.0 mw	1.5	100 ma	1.8 mw	1.1
SSL 55C	LED	0.2	14.0 mw	1.5	300 ma	4.2 mw	2.5
PR 16	Tungsten	0.46	2.7 MSCP[+]	12.5	250 ma	0.24 lm	2.0
330	Tungsten	0.23	0.5 MSCP	14.0	80 ma	0.044 lm	0.37
631	Tungsten	0.774	6.0 MSCP	14.0	630 ma	0.5 lm	4.5
1003	Tungsten	0.774	15.0 MSCP	12.8	940 ma	1.3 lm	11.0
1073	Tungsten	1.04	32.0 MSCP	13.8	1,800 ma	2.8 lm	23.0
2600[X]	Halogen	0.18	2.9 CP	3.5	720 ma	0.26 lm	2.2
3026[X]	Halogen	0.26	20.0 CP	6.3	2,100 ma	1.7 lm	15.0
1984	Q Halogen	0.38	115.0 CP	13.0	5,400 ma	10.0 lm	85.0
1966	Q Halogen	0.50	125.0 CP	13.0	7,700 ma	11.0 lm	93.0
6333[X]	Q Halogen	0.50	250.0 CP	12.0	8,300 ma	25.0 lm	210.0

[+] f/3 Optics

[X] Life less than 100 hours

[*] .6 ma/mwatt or 8.5 ma/lumen

[+] MSCP = Mean Spherical Candlepower

collect about 30% of the output of the LED and 0.7% of the output from the tungsten lamp. Lamps are available which are no larger in size than the LEDs (0.2 in. diameter) but the 330 lamp gives only 1/3 the photocurrents of the LEDs.

The PR16 lamp (an automobile spotlight lamp) gives about the same performance as the best LED with about the same current consumption, but it is larger (0.46 in. diameter). The other conventional lamps listed all have considerably more output, at the expense of higher power consumption, and are probably too large to use in an airborne OCV. However, they might prove valuable in other applications.

The halogen cycle lamps are much smaller than conventional lamps, but do not have any greater efficiency. In addition, their lifetime tends to be very short and the envelope temperature reaches 750°F, presenting a heat problem. However, the 100-watt lamp is able to generate about 100 times more photocurrent than an LED.

The LED still appears to be the best light source for an airborne OCV. Conventional tungsten lamps tend to be too bulky and draw excessive current, and the halogen cycle lamps have too short a lifetime and an excessive bulb temperature.

2. Low Pressure Discharge Lamps

Other light sources considered were low pressure and high pressure discharge lamps. Low pressure discharge lamps are very compact; their quartz envelopes have a diameter of 1/4 in. and are 2 1/8 in. long. They consume up to 17 ma of current at 270 volts. The lamps can be filled with Argon, Krypton, Neon, Xenon, or Mercury-Argon mixtures; different wavelengths are generated with the different mixtures. The Mercury-Argon lamp

is the most efficient, but generates most of its light in the ultraviolet, where silicon photodiodes are relatively insensitive. The equivalent photocurrent of this lamp with f/3 optics for collimation is only .07 when computed on the same basis as Table A.1. This compares very poorly with the LEDs. In addition, the source size is very large (3/16 x 2 in.), which would increase the size of the optical system.

3. High Pressure Discharge Lamps

High pressure discharge lamps are very large and consume considerable electrical power (from 75 to 2,500 watts); they are also very expensive (from $1.5k to $6k). Thus, they are unsuitable for a miniature airborne OCV. However, these lamps do have very small arcs and can be used with very fast f/0.7 collimating optics. A relative photocurrent of 1,000 can be obtained with a 150-watt Xenon lamp.

REFERENCES

D. Kim and G. DuBro, 1974, "The Optical Convolution Velocimeter" presented at the second Project Squid Workshop, Purdue University, Lafayette, Indiana, March 26-27.

M. Rudd, 1975, "The Optical Convolution Airspeed Indicator," Technical Report AFFDL-TR-75-125, November.

A. Fage and V.M. Falkener, 1935, "Notes on Experiments on the Temperature and Velocity in the Wake of a Heated Cylindrical Obstacle," Proceedings of the Royal Society, Vol. 135A, pp. 702-705.

A.A. Townsend, 1947, "Measurements in the Turbulent Wake of a Cylinder," Proceedings of the Royal Society, Vol. 190A, pp. 551-561.

A.A. Townsend, 1949, "Momentum and Energy Diffusion in the Turbulent Wake of a Cylinder," Proceedings of the Royal Society, Vol. 197A, pp. 124-140.

A.A. Townsend, 1948, "Local Isotropy in the Turbulent Wake of a Cylinder," *Australian Journal of Scientific Research*, Vol. 1A, pp. 161-174.

A.A. Townsend, 1949, "The Fully Developed Turbulent Wake of a Circular Cylinder," *Australian Journal of Scientific Research*, Vol. 2A, pp. 451-468.

Anatol Roshko, 1954, "On the Development of Turbulent Wakes from Vortex Streets," NACA Report 1191.

Anatol Roshko, 1960, "Experiments on the Flow Past a Cylinder at Very High Reynolds Number," *Journal of Fluid Mechanics*, Vol. 10, pp. 345-356.

John S. Humphreys, 1960, "On a Circular Cylinder in a Steady Wind at Transition Reynolds Number," *Journal of Fluid Mechanics*, Vol. 9, pp. 603-612.

D.J. Tritton, 1959, "Experiments on the Flow Past a Circular Cylinder at Low Reynolds Numbers," *Journal of Fluid Mechanics*, Vol. 6, pp. 547-567.

Mahinder S. Uberoi and Peter Freymuth, 1969, "Spectra of Wakes Behind Circular Cylinders," *The Physics of Fluids*, Vol. 12, pp. 1359-1363.

A.A. Townsend, 1976, *The Structure of Turbulent-Shear Flow* (2nd edition) Cambridge University Press, Cambridge, England.

J.S. Bendat, 1958, *Principles and Applications of Random Noise Theory*, John Wiley and Sons, New York.

S. Goldstein (ed.), 1965, *Modern Developments in Fluid Dynamics*, Dover Publications Inc., New York.

Hilpert, 1933, Forsh. Ingwes 4, and 1932 Ver. Deutsch Ing. Forshungsheft., quoted in S. Goldstein, ibid.

☆ U. S. GOVERNMENT PRINTING OFFICE: 1977 — 757-001/251